2009

Controlled synthesis of ZnO nanowires towards the fabrication of solar cells

Dongshan Yu
Virginia Commonwealth University

CONTROLLED SYNTHESIS OF ZNO NANOWIRES TOWARDS THE FABRICATION OF SOLAR CELLS

A Thesis submitted in partial fulfillment of the requirements for the degree of Master of Science in Engineering at Virginia Commonwealth University.

by

DONGSHAN YU
Bachelor in Engineering, XiDian University, China, 2007

Director: JAMES T. MCLESKEY, JR. PH.D.
DEPARTMENT OF MECHANICAL ENGINEERING

Director: CURTIS TAYLOR. PH.D.
DEPARTMENT OF MECHANICAL ENGINEERING

Virginia Commonwealth University
Richmond, Virginia
May 2009

Acknowledgement

This work would not have been possible without the encouragement and support of my advisors Dr. Curtis Taylor and Dr. James T. McLeskey, Jr., I would also like to thank all people who have helped and inspired me during my master study.

I especially would like to express my deep and sincere gratitude to my advisor, Dr. Curtis Taylor, under whose supervision I choose this topic and began the research and thesis. Dr. Taylor has provided all the benefits about conducting research, inspiring me to do the independent work, improving my presentation and academic English writing skills. His perpetual energy and enthusiasm in research had motivated me. In addition, he was always accessible and willing to give me some suggestions on every single progresses of my project. As a result, research became smooth and rewarding for me.

I was delighted to interact with Dr. James McLeskey, Jr. by having him as my co-advisor. His insight to fabrication of photovoltaic devices is second to none. He has been abundantly helpful in assisting me about experiments towards my research goals. He explained things clearly and simply. With his inspiration and great efforts, my research steps always kept in the right track. Throughout my thesis-writing period, he provided sound advice, good teaching and lots of smart ideas. I would like to express my gratitude to him for all his sincere assistance.

I wish to express my warm and true thanks to my friend and colleague, Dr. Tarek Trad. When I first enrolled in this program, he was a postdoctoral research associate in Dr. Taylor's group and my immediate research advisor. He brought me into the field of nanotechnology and taught me lots of hands-on experiences. He gave me important

guidance during my first step into self-assembly of low-dimensional nanostructures and material characterization techniques. The ideas and experiences have had a remarkable influence on my entire study in the field of nanotechnology research.

All my lab buddies at department of mechanical engineering made it a convivial place to work. They had inspired me in research and life through our interactions during the long hours in the lab. Dr. Chunya Wu, Eddie McCumiskey, Yezuo (Maverick) Wang, Shinobu Nagata, Shane Olson, Marshall Sweet, Ezzat Elshazly, and Jiancheng (Ken) Chen to be mentioned here.

I cannot end without thanking my relatives in United States, on whose constant encouragement and love I have relied throughout my time at VCU. My aunt Ningning Peng, my cousin Alex Peng, and my uncle Peter Liao.

Lastly, and most importantly, I wish to thank my parents, Tianchong Yu and Xin Peng. They gave my birth, raised me, taught me, encouraged me and loved me. They always believe their son is capable to pursue a higher education in United States without any doubt. To them I dedicate this thesis.

Table of Contents

List of figures

Abstract

CONTROLLED SYNTHESIS OF ZNO NANOWIRES TOWARDS THE

FABRICATION OF SOLAR CELLS

By Dongshan Yu, Master of Science

A Thesis submitted in partial fulfillment of the requirements for the degree of Master of Science in Engineering at Virginia Commonwealth University.

Virginia Commonwealth University, 2009

Major Directors: Dr. Curtis Taylor & Dr. James T. McLeskey, Jr.
Department of Mechanical Engineering

In recent years, quasi-one-dimensional materials have attracted a lot of research attention due to their remarkable properties, and their potential as building blocks for nanoscale electronic and optoelectronic devices. A modified chemical vapor deposition (CVD) method has been used to synthesize ZnO nanowires. Electron microscopy and other characterization techniques show that nanowires having distinct morphologies when grown under different conditions. The effects of reaction parameters including reaction time, temperature, carrier gas flow rate, substrates and catalyst material upon the size, shape, and density of ZnO nanowire arrays have been investigated.

Excitonic solar cells —including Gratzel-type cells, organic and hybrid organic/inorganic solar cells—are promising devices for inexpensive, large-scale solar energy conversion. Hybrid organic/inorganic solar cells are made from composites of conjugated polymers with nanostructure metal oxides, in which the polymer component serves the function of both light absorber and hole conductor, and the ZnO nanowire arrays act as the electron conductors. Organic solar cells have been fabricated from environmentally friendly water-soluble polymers and ZnO nanowire arrays.

Chapter 1 Introduction and Motivation

1.1 Motivation

Nanostructures have received steadily growing attentions due to their unique properties as compared to their bulk counterparts. Generating such minuscule structures is important for modern science and technology. One-dimensional (1D) nanostructures such as nanowires have attracted intensive research interests. It is generally accepted that the dimensionality and size reduction (quantum confinement) of 1D nanostructures have significant impact upon their electrical, mechanical and optical properties. [1]

Zinc oxide (ZnO) is a *II-VI* compound semiconductor with a wide bandgap (3.4eV) at room temperature. Recently, it has received a lot of attention due to its unique properties and wide applications in fabricating electronic [2], optoelectronic [3], electrochemical and electromechanical devices of nanoscale dimensions. [4]

Size-controlled synthesis of ZnO nanowires has made the application of nanowire arrays to organic solar cells possible [5]. Since the discovery of polyacetylene in 1977, conductive conjugated polymers have been widely utilized in photovoltaic devices [6], light-emitting diodes [7], transistors and sensors [8]. Polymer based solar cells can greatly reduce the manufacturing cost via inexpensive liquid based processing techniques such as spin coating, doctor blading, ink jet printing. However, the performance of the solar cells made from homogenous polymer layers has been limited due to their low charge mobility and short exciton diffusion length. Many studies have been carried out to solve this crucial problem by building bilayer and bulk heterojunction structures with the phase separation between the polymer and inorganic nanostructures such as TiO_2 nanoparticles

[9] and ZnO nanowires [5]. To maintain efficient charge separation in nanowire-based architecture, the nanowires must be thin (diameter less than 50 nm) and closely spaced, with a wire-to-wire distance equal to approximately twice the diffusion length of exciton in the polymer, which is usually 5-20 nm. A dense and evenly distributed ZnO nanowire array will provide a direct path for photogenerated electrons traveling to the collecting electrodes therefore improve the device energy-conversion efficiency. In order to apply the zinc oxide nanowire to the field of photovoltaic devices, a technique, which allows for repeatable and predictable synthesis of nanowires with atomic-level control of size, shape, position and composition, needs to be developed. Vapor-Liquid-Solid process (VLS) is one of the most effective ways for nanowire synthesis and offers a potential solution for the problem.

The morphology and density of as-synthesized nanowire arrays are determined by the factors including reaction time, temperature, carrier gas flow rate and the type of substrate and catalyst. However, there are several problems that remain unresolved.

(1) In CVD synthesis of ZnO nanowires, there are several controllable parameters. The morphology of the as-synthesized nanostructure is determined by those parameters. Therefore, a parametric investigation of the effect of each factor upon the size and shape of nanostructure is needed.

(2) A dense and evenly distributed nanowire array is required for application to photovoltaic devices application. Therefore, the growth positions of nanowires should be rationally controlled through the CVD growth process. The wire-to-wire spacing should be uniform and optimized for carrier diffusion.

(3) Photo-generated excitons are strongly bound and resist dissociation into separate charges in polymers. This problem is often addressed by building bilayer heterojunction structures with phase separation between the polymer and certain inorganic nanostuctures. The interface between the polymer and the inorganic material must be good. The polar nature of the ZnO may make it suitable for use with a water-soluble polymer (PTEBS). The performance of solar cells made from ZnO nanowires and water-soluble polymer bilayer heterojunction is measured to evaluate this idea.

1.2 Objectives

The primary objective of this investigation is to determine the effects of reaction conditions on the size, shape and density of as-synthesized zinc oxide nanowires. A parametric study of the effect of temperature, time, gas flow rate and catalyst material on the morphology and density of the nanowire array has been conducted. The aim of this part of study is to determine the optimal reaction conditions for zinc oxide nanowires synthesized via the Chemical Vapor Deposition (CVD) method. In addition, seed-layer assisted synthesis of zinc oxide nanowire arrays has also been investigated. The use of ZnO growth seeds can lead to better alignment of the ZnO nanowire on the substrate due to the epitactic relationship. Zinc oxide nanowires were synthesized via hydrothermal solution at low temperature on substrates coated with zinc oxide seed layer. Various material characterization techniques including Scanning Electron Microscopy (SEM), Energy dispersive spectroscopy (EDS) have been utilized to characterize the morphology of the ZnO nanowire produced through each method.

A secondary objective is to determine whether the novel solar cells made using zinc oxide nanowire arrays and water-soluble polymers can achieve power conversion efficiencies equal to or even better than those made with conventional polymers and metal oxide materials. This is the first study of incorporating the zinc oxide nanowire with the organic solar cells made from a water-soluble polymer. The water-soluble thiopene polymer, sodium poly[2-(3-thienyl)-ethoxy-4-butylsulfonate] [PTEBSNa], was used to build photovoltaics by incorporating ZnO nanowires to create bilayer solar cells.

Devices were fabricated in a bilayer configuration and a significant photovoltaic effect was observed.

Chapter 2 Zinc oxide nanowire synthesis and characterization

2.1 Zinc oxide nanowires: properties, importance and applications

2.1.1 Crystal structure and chemical bonding of Zinc Oxide

Zinc oxide (ZnO) is an *II-VI* compound semiconductor. It has a direct and wide band gap of 3.37 eV at room temperature with a large exciton binding energy (60meV) and an exciton Bohr radius in the range of 1.4-3.5 nm. It occurs in nature in the form of a mineral named zincite. Usually, other elements such as manganese are contained in zincite mineral which make it appears red or yellow color. [10]

Zinc oxide preferentially forms a hexagonal wurtzite-type crystalline structure with lattice parameters a=0.3296 and c=0.52065 nm. The resulting c/a ratio has a value of around 1.60, slightly different from the ideal value c/a=$\sqrt{8/3}$=1.633. [10] The c axis is parallel to z. The wurtzite structure can be described as a numbers of alternating tetrahedrans composed of coordinated O^{2-} and Zn^{2+} ions, stacked alternately along the c-axis (Figure 1). One zinc ion is surrounded by four oxygen ions in a tetrahedral unit cell and vice versa. This non-central symmetric structure results in piezoelectricity and pyroelectricity properties. [10]

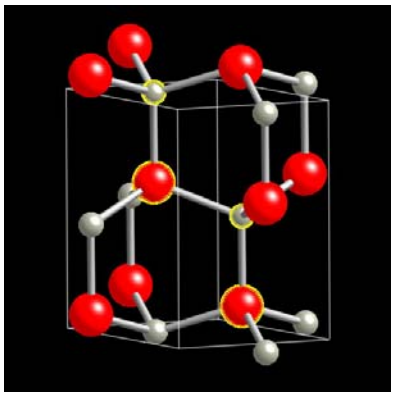

Figure 1.The crystal structure of ZnO [11]
(Zn white, O red; highlighted atoms are inside unit cell)

Polar surfaces are another important characteristics in the ZnO wurtzite structure. [12] Spontaneous polarization along the c-axis and a normal dipole moment is produced by oppositely charged Zn-(0001) and O-$(000\bar{1})$ surfaces. The polar surfaces also result in divergence in surface energy. [12 Usually, the polar surfaces have facets for exhibiting surface reconstruction to maintain a stable structure. However, the planes ± (0001) in ZnO wurtzite structure are atomically flat, stable and without reconstructions. The reason for the stability of ZnO is still not fully understood and currently at the forefront in surface physics research.

2.1.2 The importance of nanoscale science and technology

The word "nano" refers to a reduction of size or time by 10^{-9}, which is a million times smaller than a millimeter. A nanometer is equal to 10^{-9} meter and it is 10,000 times smaller than the diameter of a human hair. Nanoscience, nanoengineering and nanotechnology all deal with small sized systems and objects. The official definition of nanoscience/nanotechnology from United States National Science Foundation is studies that deal with both materials and systems having the following key properties [13]:

(1) Dimension: at least one dimension from 1 to 100 nanometers (nm).

(2) Process: designed with methodologies that show fundamental control over the physical and chemical attributes of molecular-scale structures.

(3) Building block properties: they can be combined to form larger structures.

The essence of the nanoscale science and technology is based on the fact that the material properties (i.e. chemical, magnetic, electrical, mechanical, and optical) in nanoscale have significant differences from those in the bulk, enabling unique applications. For example, opaque substances become transparent (copper); stable materials turn combustible (aluminum); solids turn into liquids at room temperature (gold); insulators become conductors (silicon). A material such as gold, which is chemically inert at normal scales, can serve as a potent chemical catalyst at nanoscale. These properties are intermediate between properties of atoms or molecules from which they are composed and those of macroscopic materials. It has been demonstrated that nanoparticles have enhanced performance properties compared to bulk materials when they are used in similar applications. The quantum mechanical wavelike properties of electrons vary from those in macroscale. Nanoscale design gives rise to the possibility to vary material's micro and macroscopic properties, such as charge capacity, magnetization and melting temperature, with the unchanged chemical composition. [14] Furthermore, the high surface to volume ratio makes the nanoscale components ideal for use in composite materials, reacting systems, drug delivery, and chemical energy storage (such as hydrogen and natural gas) [15].

Recently, one dimensional nanostructures including nanorods, nanowires, nanobelts and nanotubes have been studied extensively due to their unique properties and the potential to revolutionize the area of nanotechnology. First of all, the one dimensional

nanostructures are the smallest structures for electrical carrier transport. Therefore they can be integrated in nanoscale systems for moving charges. In addition, one dimensional nanostructures can be built as wiring and device elements in functional nanosystems. Currently, carbon nanotubes and semiconductor nanowires are the two promising materials in this regard. [15]

Single-walled carbon nanotubes (NTs) are allotropes of carbon with a length-to-diameter ratio of up to 28,000,000:1. [15] Depending on their diameter and helicity, NTs can exhibit either metallic or semiconductor behavior. [15] The unique electronic properties render the possibility of making different devices which could be used in nanoelectronics. Recently, NTs have been used to fabricate room-temperature field effect transistors (FETs) [16], diodes [17] and logic circuits [18]. However, it is hard to determine whether the NT building blocks exhibit semiconductor or metallic behavior, and device fabrication usually is a random event. A solution to this problem involves selective destruction of metallic tubes, although such an approach requires extensive top-down lithography and subsequent processing.

Semiconductor nanowires (NWs) are another important nanostructure. In contrast to NTs, the size, interfacial properties, and electronic properties can be predictably and precisely controlled by several key parameters during synthesis [19]. Therefore, it enables a wide-range of device applications and integration methods in rational manner. For example, semiconductor NWs building blocks can be integrated into nanoscale p-n diodes [20], FETs [21], complex logic gates [22], complementary inverters [21] and even computational circuits [22] Moreover, it is possible that distinct NW building blocks can be combined together in ways not possible in conventional electronics. As a result, the

semiconductor NW devices may achieve new functionality and could lead to unexpected device concepts.

2.1.3 Physical properties of ZnO nanowires

Zinc oxide is a wide band-gap semiconductor with band gap energy of 3.37 eV. Some of the physical properties of bulk ZnO are listed in the following table. [1]

Table 1. Physical properties of wurtzite ZnO

Properties	Values
Lattice constants (T=300K) a_0	0.32469 nm
Lattice constants (T=300K) c_0	0.52069 nm
Density	5.606 g/cm^3
Melting point	2248K
Relative dielectric constant	8.66
Band gap energy	3.4 eV, direct
Intrinsic carrier concentration	$<10^6$ cm^{-3}
Exciton binding energy	60 meV
Electron effective mass	0.24
Electron mobility (T=300K)	200 cm^2/Vs
Hole effective mass	0.59
Hole mobility (T=300K)	5-50 cm^2/Vs

Understanding the basic physical and chemical properties of ZnO nanostructure is important in developing nanostructure based building blocks for future nanoscale devices. As the dimension of semiconductor materials like zinc oxide shrinks down to nanometer

scale, their properties will be changed as described as “quantum size effect”. It has been proven by photoluminescence that the band gap energy of quasi-one-dimension (Q1D) ZnO increases due to the quantum confinement. [23] Studies of scanning photoelectron microscopy and X-ray absorption have also demonstrated the enhancement of surface states with the minimizing of ZnO nanorods. [24] Furthermore, based on the research of nanowires used in chemical sensing studies, the carrier concentration in Q1D systems can be changed by the surface states. [25] One-dimensional ZnO nanowires can also be used as building blocks to assemble nanoscale electronic circuits and photonics in future.

2.1.3.1 Mechanical properties

Since the traditional measurement methods for mechanical characterization of bulk materials are quite challenging to apply in nanostructures, direct measurement of the mechanical properties of zinc oxide nanowires have attracted lots of attention. The lattice defects often lead to mechanical failure. The single-crystalline zinc oxide nanostructures are supposed to be significantly stronger than their counterparts that have larger dimensions due to a reduction in the number of defects per unit length. X.D.Bai *et.al.* [26] developed an experimental approach based on the electric-field-induced resonant excitation for directly measuring the mechanical properties of nanowire structures using *in situ* TEM. The fundamental resonance frequency of zinc oxide nanowire can be calculated from the classical elasticity theory: $v = \frac{\beta_i^2 T}{4\pi L^2}\sqrt{\frac{E}{3\rho}}$ Where β_i is a constant for the i th harmonic: β_1=1.875 and β_2=4.694. E is the bending modulus for the vibration along the longitudinal direction. L is the length of the nanowire, ρ is mass density. Based on the experimentally measured data, the bending modulus of the zinc oxide nanowire is calculated using the equation above. The bending modulus of the zinc oxide nanowire is

~52 Gpa. The single crystalline nanowires could be used as a type of nanoresonator [27] and nanocantilever [28], which could be useful in nano-electro-mechanical systems.

2.1.3.2 Electrical properties

The single crystalline structure gives the ZnO nanowire superior electrical properties as compared to polycrystalline thin film. It has been proven that the electron field mobility of single crystalline ZnO nanowire can be as high as 80 $cm^2/V \bullet s$, which is almost ten times than that of ZnO thin film transistors. [29]Furthermore, Park *et al.* have demonstrated that the electron mobility of a ZnO nanowire can reach to 1000 $cm^2/V \bullet s$ after it is coated with polyimide in order to reduce the electron trapping and scattering at surface. [30] That means the ZnO nanowires have the potential to be applied into nanoscale devices with a significant improvement in operation speed.

The difficulty of *p*-type doping is a major obstacle towards using ZnO nanowires in electronics and photonics devices. The potential for applying ZnO nanowires into future nanoscale electronic and mechanical devices will be greatly enhanced if successful *p*-type doping can be achieved. Nowadays, several cases of *p*-type doping have been reported. Look *et al.* developed a Ga and N codoping by molecular beam epitaxy providing an electron hole mobility of 2 $cm^2/V \bullet s$. [31] Kim *et al.* reported phosphorus-doped *p*-type ZnO nanowire utilizing thermal activation process. [32] Combining the *p*-type and *n*-type ZnO nanowires together is the first step in fabricating *p*-*n* junction diodes and light emitting diodes (LED). Liu *et al.* fabricated intramolecular *p*-*n* junction diodes on ZnO nanowires. [33] In this case, they chose an anodic aluminum membrane with average pore size around 40 nm to make a porous template. They introduced boron as the

p-type dopant and a two step vapor was carried out to synthesize ZnO nanowires. As a result, the I-V curve showed rectifying behavior of *p-n* junction.

2.1.3.3 Optical properties

The intrinsic optical properties of ZnO nanowires are important for implementing photonic devices. It has a strong exciton binding energy of 60 meV and it has been proven that a significant enhancement of the exciton binding energy can be achieved by quantum size confinement. Photoluminescence (PL) has been used to observe the excitonic spectra of ZnO nanowires. [34] Three emitting bands, including a strong ultraviolet emission at 386 nm and a weak blue band (440-480 nm) as well as an almost negligible green band (510-580 nm) have been recorded for ZnO nanowires with a diameter in the range 60 to 80 nm. [1] The strong UV emission peak at 380 nm is due to the emission from conduction band to valence band. [1] A photogenerated hole may recombine with singly ionized charge state of the defect. It has been widely accepted that the green band emission is dependant on the different type of oxygen vacancies. [1]The intensity of green luminescence is proportional to the concentration of oxygen vacancies contained in ZnO nanowires. Furthermore, the thinner ZnO nanowires with their higher surface-to-volume ratio always favor a higher level of defects and surface recombination. Therefore, the ZnO nanowires with smaller diameter have stronger emission intensities [1]. In addition, a blue shift in the near UV emission peak in ZnO nanowires is observed. As one of the characteristic of nanoscale system, blue shift is caused by quantum confinement.

2.1.3.4 Piezoelectricity

Piezoelectricity is the ability of some materials to generate an electric potential in response to applied mechanical stress. The internal crystalline structure of ZnO nanowires results in their piezoelectric properties. This has been extensively studied for various applications in force sensing, acoustic wave resonators, and acousto-optic modulators. [35-36] Studies of the ZnO crystal structure reveal that four oxygen atoms with negative charge and a zinc atom with positive charges are tetrahedrally bonded. [1] The center of gravity of four oxygen atoms is at the same position of the tetrahedron. When an external force is applied to the crystal along the corner direction of the tetrahedron, a lattice distortion will occur, and as a result, the center of gravity of the four negative charges will no longer coincide with the position of the positive atom; therefore, an electric dipole is generated. [1] The crystal will have a macroscopic dipole if all the tetrahedrons in the crystal are aligned in the same crystal orientation. The two opposite faces of the crystal can be treated as opposite electrodes.

2.1.4 ZnO nanowire applications and devices

ZnO nanowires are a functional nanoamaterials, which have novel properties due to their size effect and surface effects. They have potentials applications in nanodevices in a variety of fields.

2.1.4.1 Nanowire chemical and biological sensors

Oxygen vacancies on ZnO nanowires serve as *n*-type donors and often significantly increase the conductivity of the oxide. Charge accepting molecules such as NO_2 and O_2 can be adsorbed at the vacancy site. In this case, electrons in conduction band will be depleted, resulting in a reduction in the conductivity of the *n*-type oxide. On

the other hand, CO and H_2 molecules react with oxygen adsorbed on the surface and remove it leading to an increase of conductivity. The ZnO nanowire gas sensor operates based on this principle. Extensive efforts have been made on solid state gas sensor fabrication where both bulk and thin film ZnO have been utilized CO, [37] NH_3, [38] alcohol, [39] and H_2 [40] sensing. Since the diameter of ZnO nanowire is comparable to the Debye length, the electronic structure of the entire channel is effectively affected by chemisorption induced surface states. Wan *et al.* have recently fabricated a ZnO nanowire chemical sensor for microelectromechanical system. [41] Below a certain operational temperature, the resistance of nanowires significantly decreases when the sensor is exposed to ethanol.

2.1.4.2 Field effect transistors

Native defects such as oxygen vacancies and zinc interstitials give ZnO nanowires *n*-type semiconductor behavior. The wide direct band gap, multifunctional properties, and semiconductor behavior make ZnO nanowires promising materials for nanoscale electrical devices such as diodes, field effect transistors, and chemical sensors. Cha *et al.* have fabricated a high performance ZnO nanowire FET, which has simple structure and fabrication procedure. [42] A distinct feature of their work is the use of self-aligned gates to achieve nanosize air gap capacitors. They use suspended ZnO nanowires as the starting material. The gaps between suspended nanowires and electrodes are controlled to be 25 nm. After the electron measurements, the FET showed 3.06 μS in transconductance as well as 450 cm^2/V in mobility under low voltage operation, while the gates and drain voltage are less than 1.0 V. Zhiyong Fan and Jia Lu have fabricated a Field Effect Transistor using single ZnO nanowires and characterized their electrical properties using

scanning probe microscopy (SPM). [43] In this work, individual *n*-type ZnO NW is configured as FET, and a conductive SPM is used as a movable local gate. They found that the effective Schottky barrier heights can be modified by local gating when it applied at the contact region. If the tip is applied at the middle of the nanowire, the negative tip bias causes a local negative tip bias which obstructs the electron transport. However, they also found that a positive tip gating does not affect the conductance significantly. Therefore, they demonstrate a scanning tip gating effect that the conductance of the nanowire is modulated periodically by the negatively biased scanning tip.

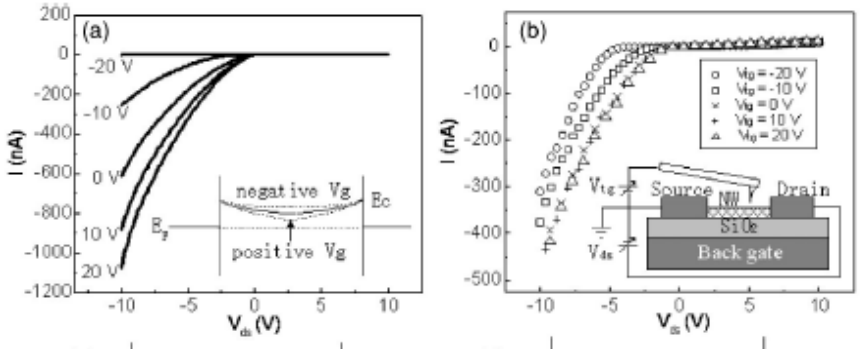

Figure 2. *I-V* curves measurements of nanowire field effect transistor (a) *I-V* curves under different back gate voltages of -20,-20, 0, 10, and 20V. Insert: A diagram illustrating band bending caused by back gating; (b) *I-V* curves under different tip gate voltages. Insert: schematic showing the circuit measurement setup[43]

Electrical transport in ZnO NW FETs illustrates how tip gating modulates the conductance in the nanowire. Figure 2(a) shows the *I-V* curves of an *n*-type ZnO NW under different back gate voltages ranging from -20 to 20 V. Conductance of nanowire significantly increases as the response of the increase of back gate voltage. The inset of Fig. 2(a) shows that the positive back gate potential increases electron concentration and bends the conduction band towards the Fermi level, thus yielding resulting in higher conductance. However, a negative back gate depletes the electron concentration, bends the conduction band away from the Fermi level, resulting in lower conductance. When

the conductive SPM tip is applied at the middle of the ZnO NW, the conductance of nanowire does not increase considerably for positive tip gate voltage (V_{tg})

2.1.4.3 Solar Cells

Zinc Oxide nanowires have also been used as the electron acceptor in solar cells. They are chosen because of their potential to improve electron transport and increase the efficiency of the devices. Since zinc oxide nanowire array provide a direct path of photogenerated electron, the electron recombination rate will be decreased in the organic solar cells made from zinc oxide nanowires. Several kinds of organic solar cells have been fabricated by incorporating zinc oxide nanowires in their architectures. Junpeng Liu *et al.* fabricated a hybrid organic/inorganic solar cell. In this device architecture, copper-phthalocyanine (CuPc) and fullerene (C_{60}) were served as donor and acceptor. The device was combined with vertically orientated ZnO nanowire arrays as direct charge transport paths to improve the device photovoltaic performance. PEDOT:PPS polymer was used as an hole-conducting layer to improve the hole conductivity. The open circuit voltage has reached to a maximum of 0.46 V and the short circuit current reached 3.86 mA/cm^2. The power conversion efficiency has reached 0.53% [44]. Dye-sensitized solar cells have been fabricated by Uasuhide Nakamura *et. al.* by incorporating zinc oxide nanowires [45]. Further details on ZnO based solar cells are given in chapter 3.

2.2 ZnO nanowire array synthesis

2.2.1 Chemical Vapor Deposition

Chemical Vapor Deposition (CVD) is a surface modification process for solid material coating. The definition of CVD was firstly appeared in literature in the 1960s. Today, it became to an important technique not only in solid thin-film surface coating, but also in producing of bulk materials and low dimensional assembly of nanostructures. In a typical CVD process, volatile precursors are transported to heated substrates, where they react and condense on the surface to make desired deposition. This process is accompanied by the production of by-products, which are pumped out of the chamber with the surplus resource gases. Several reaction parameters including: reaction temperature, carrier gas flow rate, pressure and reaction time are controllable during the CVD process to form the corresponding products. The occurrence of the chemical reaction is an essential characteristic of the CVD method [46].

The chemical reaction is generally activated thermally by resistance heat, plasma or lasers. It occurs on and near the hot surface, resulting in the deposition of a thin film on the surface. There are also many variations of the CVD. For example: Plasma-Enhanced CVD (PECVD) is a CVD processes utilizing plasma to accelerate the chemical reaction rate. The plasma is produced by RF frequency or DC discharge between two electrodes, allowing deposition at relatively lower temperature.

Chemical Vapor Deposition has a wide range of operating pressures. Most CVD is done at atmospheric pressure, which known as Atmospheric pressure CVD (APCVD). Some types of CVD are also capable of working at extremely high vacuum (usually up to

10^{-7} P), named Ultrahigh Vacuum CVD (UHVCVD). Chemical vapor deposition systems using metalorganic compounds as the sources is known as metalogranic chemical vapor deposition (MOCVD). Recently, MOCVD has been widely applied in the fabrication of GaN quantum well light emitting diodes (LEDs).

CVD has a number of advantages in depositing thin films and nanostructures. One of the primary advantages is that the solid deposited through the CVD technique is quite conformal. Another advantage of CVD is that, it is capable of depositing high quality thin films. Distillation techniques have been applied in chemical vapor deposition to remove impurities from gaseous precursors. Other advantages include relatively high deposition rates, and the fact that CVD often doesn't require as high a vacuum as physical vapor deposition [46].

Chemical Vapor Deposition has been widely used in nanocluster catalyst growth of nanowires, in which the reactant and dopants are well-defined gas sources. The nanowire size, composition and doping level can be controlled in a very precise manner via the catalytic CVD method. The size of as-synthesized nanowires is controlled by three factors: (1) the size of eutectic droplet is defined by the size of metal catalyst nanocluster; (2) the growth temperature determines the solubility of reactant in catalyst nanocluster then the size of eutectic droplets; and (3) the diameter of nanowire can be affected by the vapor pressure of the reactant when it exceeds the critical value for homogeneous deposition of reactant onto nanowire surfaces [15].

2.2.2 Vapor transport synthesis of ZnO nanowire

In general, the requirement for one dimensional nanostructure growth is that two dimensions are confined to the nanometer regime, while the third dimension can be

extended to macroscopic scale. Compared to the growth of zero dimensional and two dimensional structures, this growth is much more difficult. Lots of semiconductor materials show cubic, zinc blende crystal structure. For the early stage of crystal growth, the resulting nanoscale structures are usually three dimensional polyhedrons or nanocrystalline rather than one dimensional nanowires. If the atomic bonding is relatively isotropic, the symmetry must be broken during the growth to achieve the one dimensional structure. [15]

The vapor transport process is the most common method for physical synthesis of ZnO nanowires. Basically, powder precursor is vaporized at increasing temperature and the resultant vapor is then condensed onto the substrate to form the desired product under temperature, pressure or atmosphere changes. Several processing parameters such as temperature, pressure, and flow rate of carrying gas can be controlled during the thermal vaporization. According to the volatility of the precursor material, the reaction temperature should be a little bit lower than the melting point of the precursor. The pressure depends on the evaporation rate when the source material is vaporized. The substrates are placed downstream away from the carrier gas to collect the growth products; the local temperature of substrates usually is a crucial factor for the nanostructure growth; it determines the type of product deposited on the substrate. Another crucial factor for nanostructure deposition is the appearance of oxygen. It has been provn that the concentration of oxygen in growth system can affect thermal evaporation process, [10] not only the volatility of the precursor, but the stoichiometry of the vapour phase and the formation of the final products.

The vapor transport process can be categorized into the catalyst free vapor-solid (VS) process and catalyst assisted vapor-liquid-solid (VLS) process. In VS process, precursor in vapor phase is condensed to form a rich variety of nanostructures including nanorods, nanowires, nanobelts and other complex structure. However, it has less control over the geometry, alignment and location of as-synthesized nanostructure. In catalyst-assisted VLS process, the crystal growth is promoted by the presence of liquid alloy-solid interface (Fig.3). Vapor-liquid-solid nanowire growth mechanism includes three stages: alloying, nucleation and axial growth as shown in the figure below.

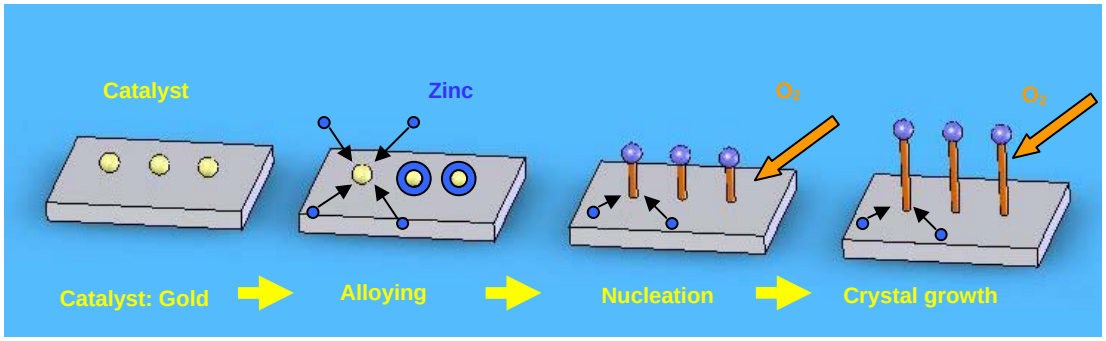

Figure 3. Schematic of Vapor-Liquid-Solid process of zinc oxide growth

The catalyst is an important factor in VLS process since the growth of nanostructures takes place in the catalyst droplets. The catalyst is usually a metal nanocluster or nanodroplet. Various nanoparticles or nanoclusters have been selected as catalysts, including Au, Cu, Co, and Sn. In the VLS process, vapors of zinc and oxygen mixture are transported and reacted with each other. The gaseous reactants are absorbed by the liquid catalyst alloy cluster since the sticking coefficient is much higher on liquid versus the solid surface. The one dimensional growth is mainly controlled by the liquid droplet, the size of which remains unchanged during the entire growth process. When supersaturated, the 1D growth starts from the solid-liquid interface of the alloy droplets

where the surface energy is minimized. The 1D growth continues in the presence of reactant by pushing the liquid-solid interface forward as long as the catalyst nanodroplet remains in the liquid state. One feature of nanowires synthesized from VLS process is that each nanowire is capped with a nanoparticle. Based on this mechanism, the diameter of each nanowire is largely determined by the size of catalyst, smaller catalysts should yield thinner nanowires. According to the diameter of the nanoscale catalyst cluster, nanostructures with appropriate size can be rationally synthesized.

A modified Chemical Vapor Deposition (CVD) process used to synthesize the n-type ZnO nanowires without incorporating impurity dopants has been reported by Chang *et al.*[29] Native defects in zinc oxide crystal structure, such as zinc interstitials and oxygen vacancies, give the ZnO *n*-type semiconducting behavior, and these defects serve as electron donors. With the vapor trapping CVD method, the crystal defects were intentionally introduced into the nanowires via the synthesis process.

In order to introduce more native defects, a quartz vial was placed in the quartz furnace tube to maintain a zinc-rich environment; the configuration of the system is shown as follows:

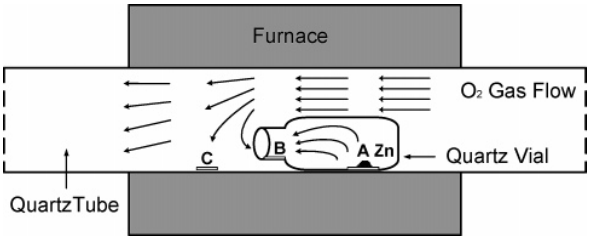

Figure 4. Schematic illustration of the CVD system with a inlet quartz vial placed inside of furnace tube[25].

Since the quartz vial was placed downstream of the carrier gas flow, zinc vapors diffuse away slowly from the vial compared to oxygen vapor; therefore, the high zinc

vapor concentration is maintained inside of the vial, creating a rich zinc concentration condition with dilute oxygen.

Silicon (Si 001) chips were used as substrates in this experiment. As shown in Figure 4. Chip A was placed close to the bottom of the quartz vial, Chip B was placed at the bunghole, and Chip C was placed 2.5 cm away from the vial. The synthesis was carried out at 700^{o}C for 10 min with a constant Ar gas flow of 90 sccm. SEM image showed that nanowires were distributed uniformly on Chip C with diameter ranging from 20 to 200 nm, and the average length is about 30 μm [40]. For Chip B, ZnO crystals in various geometrical shapes have been produced at different area of the substrate. High-quality nanowires were grown at the central area of the substrate. The highest quality nanowires synthesized on Chip B have diameters from 20 to 300 nm and average length of 20 μm [29].

The conclusion is that the vapor pressure difference between zinc and oxygen is critical for nanowire growth. The morphology of the ZnO nanowire crystal is determined by the relative rate of surface reaction with respect to the mass transfer rate of zinc and oxygen vapor.[29] The electronic properties for ZnO nanowire synthesized through this method are also investigated. By comparing the electrical transport properties between the nanowires synthesized by this method and the one synthesized by traditional VLS method, the author claimed that the *n*–type behavior of ZnO nanowires can be synthesized via chemical vapor deposition process. The synthesized zinc oxide nanowires also have higher carrier concentration and better conductivity [29].

2.2.2 Wet-chemical synthesis method

Chemical Solution Deposition (CSD) is a highly effective and competitive alternative to vapor transport technique. It refers to chemical deposition in the liquid phase. The traditional vapor-phase transport process with the assistance of metal catalysts, thermal evaporation and template-assisted growth for synthesizing one-dimensional ZnO nanostructures have some innate disadvantages. The introduction of catalysts and templates may result in impurity at final products and involves a much more complicated experimental process at the same time when compares to chemical synthesis methods. Besides, the nanowires and nanorods prepared by VLS growth process may entangled together and bundles may form with some junctions [48]. In these cases, the nanostructures are not evenly distributed at the substrate either. It will limit their practical applications in building nano-devices. Therefore, the wet chemical approach of ZnO nanostructures synthesis is a promising option for the large-scale production of well-dispersed materials.

Solvothermal synthesis has been widely used for nanowire synthesis. In order to speed up the reactions between solids and increase the solubility of solids, the solvent is prepared under pressures and temperature above its critical point. In a typical procedure, a solid precursor and reagent are added into a solvent with appropriate ratio. Then the mixture is placed in a sealed environment with elevating temperature and pressure to allow the reaction occurs and nanowire growth. Heath and co-workers reported the use of solvothermal synthesis for nanowire synthesis. [47] They reduced $GeCl_4$ or phenyl-$GeCl_3$ with sodium in an alkane solvent heated and pressurized to 275^{o}C and 100 atm (just above the critical point) to synthesize Ge nanowires. Single-crystalline nanowires of 7-30 nm in diameter and up to10 μm in length have been obtained through this method. Jinmin

Wang and Lian Gao have reported the synthesis of ultralong and straight single-crystalline ZnO nanowires by a simple hydrothermal treatment of the zinc carbonate hydroxide hydrate ($Zn_4CO_3(OH)_6 \cdot H_2O$). [48] The growth direction was [0 1 -1 0], and the single-crystalline ZnO nanowires had average diameters of 80-100 nm and lengths of over 10μm.

2.2.3 Patterned growth and vertical alignment of ZnO nanowires arrays

The patterned growth of ZnO nanowires is important to their future application. The location, alignment and packing density of ZnO nanowires can be controlled through the synthesis process. Lithographic and non-lithographic patterning techniques have been utilized to control the location of ZnO nanowires. In photolithographic techniques, [49] nanoindentation is utilized in making square and hexagonal catalytic gold dot arrays on the substrate, then the nanowires are grown form the patterned catalyst via VLS process.

Another simple alternative for creating patterned catalysts array is the use of shadow masks to deposit catalyst films. Usually, TEM grids are used to make square Au matrix patterns. [50] Other advanced lithography techniques such as electron beam lithography have also been utilized to create well-ordered shadow mask. Anodic aluminum oxide membranes (AAM) have been utilized by Chik *et al.* as a mask to create Au catalyst patterns to fabricate hexagonal ZnO nanowires arrays on GaN substrates. [51] As a result, highly ordered ZnO nanowires arrays have been grown at the hexagonal catalyst dot sites.

The growth orientation of ZnO nanowires can also be controlled via lithographic patterning technique. Vertically aligned ZnO nanowires/nanorods have potential in

making electron field emitters [52], organic solar cells [59] and UV lasers [53]. Ng *et al.* developed ZnO nanowire-based vertical field effect transistors with surround gates. [54] They developed the vertical aligned ZnO nanowires which were grown from lithographically patterned Au spots. They deposited SiO_2 and Cr around the nanowires to serve as the gate oxide and gate electrode.

Lattice matching between ZnO and the substrate is another important factor in generating the vertical aligned nanowire. Wenjie Mai et.al synthesized vertically aligned ZnO nanowires on several semiconductor substrates such as sapphire, GaN, SiC, and Si. [55] The demonstrated that the vertically aligned ZnO nanowire arrays (wurtzite, a=0.3249 nm, c=0.5207 nm) can be found at SiC (0001) (wurtzite, a=0.3076 nm, c=0.5048 nm) and GaN (0001) (wurtzite, a=0.3189 nm, c=0.5185 nm) substrates. The ZnO (0001) plane has a relatively small lattice mismatch (less than 6%) with the SiC (0001) and the GaN (0001) planes. Vertically aligned ZnO nanowire arrays grow favorably at these substrates in a heteroepitaxial growth process. It has been well accepted that ZnO nanowires favor to grow in a direction which associate with lowest surface energy, especially at their nucleation and initial growth stage. Therefore, the 0001 plane is the fastest growth direction for ZnO nanowires in the VLS process. If it is not the boundary of lowest energy, the fasted growth direction for ZnO nanowire could be a random direction, the percentage of vertically aligned nanowire will be significantly reduced.

Yang *et al.* reported the growth of vertically aligned ZnO nanowires on sapphire $(11\bar{2}0)$ plane. [52] They also proved that the lattice mismatch between ZnO and the substrate determined the quality of vertically alignment of ZnO nanowires. Fan *et al.* compared the quality of vertical aligned ZnO nanowires grown on both GaN and sapphire

substrates. [50] Because GaN has the similar lattice constants and the same crystal structure with ZnO; it is a suitable substrate for growing vertically aligned ZnO nanowire. SEM images showed that the ZnO nanowires grown on GaN epilayer had better vertical alignment than the counterparts grown on sapphire.

2.3 Material characterization techniques

2.3.1 Introduction to scanning electron microscopy (SEM)

Scanning electron microscopy (SEM) is an important material characterization approach. It takes images from the sample surface using a high-energy beam of electrons. The electron beam scans across the sample surface and interact with the atoms to produce signals regarding to the sample's surface topography. Several signals can be produced by SEM, which are secondary electrons; back scattered electrons, characteristic X-rays, light (cathodoluminescence), specimen current and transmitted electrons. In a standard detection mode, back-scattered electrons (BSE), which are beam electrons that reflected from the sample by elastic scattering [56], are used for SEM imaging. According to the DeBroglie equation, The velocity of an electron accelerated through 100 volts in SEM is 5.9×10^6 m/s. According to DeBroglie equation, the DeBroglie wavelength can be calculated as: $\lambda = \frac{h}{mv} = \frac{6.626 \times 10^{-34} J \bullet s}{(9.11 \times 10^{-31} kg)(5.9 \times 10^6 m/s)} = 1.2 \times 10^{-10} m$, which is almost 3000 to 6000 times smaller than that of visible light ($3.9 \times 10^{-7} \sim 7.8 \times 10^{-7}$ m)[56]. Therefore, SEM is capable of characterizing sample surfaces with extremely high-resolution (up to 1 to 5 nm) through the BSE imaging. It also yields a wide range of magnifications, ranging from 25 times to 250, 000 times, which is approximately 250 times higher than magnification limit of the light microscopes. In addition, with a very large depth of field, SEM is capable for characterizing the sample surface in three dimensions, which is useful to reveal the surface topography.

2.3.2 Introduction to energy dispersive X-ray spectroscopy (EDX)

Energy dispersive X-ray spectroscopy (EDX) is an analytical technique for the elemental analysis or chemical characterization of an unknown sample [57].When charged particles hit the sample; analyzing x-rays are emitted in response to the collision between the charged particles and sample atoms. Through investigation of the interactions between electromagnetic radiation and the matter, chemical composition of the matter is analyzed. Because characteristic x-rays are unique for each element, it can be used to identify the unknown material.

EDX systems are usually installed on scanning electron microscopes (SEM-EDX). The high energy electron beam is focused into the sample for SEM imaging and stimulates the emission of characteristic x-rays at the same time. Ground state electrons in discrete energy levels are contained in an atom at rest. An electron in an inner shell might be excited by the incident electron beam; the excited electron is then jumped into the higher energy shell, leaving an electron hole. Then the hole is filled by an electron from an outer, higher-energy shell. An x-ray will be released when there is an energy difference between the higher-energy shell and the lower energy shell. An energy dispersive spectrometer is equipped in the EDX system; it is capable of analyzing the number and energy of the X-rays emitted from a specimen. As the difference in energy between the two shells is unique for each element, the X-ray is characteristic for the atomic structure of the element form which they were emitted. Therefore, the elemental composition of the specimen is measured.

In a typical SEM-EDX system, a cathode and magnetic lenses are equipped to stimulate and focus a beam of electrons into the sample surface. X-ray energy is

converted into voltage signals by a detector; this signal is analyzed by a pulse processor to determine the chemical composition.

Chapter 3 Introduction to Solar Cell

3.1 Characteristic of solar cells

3.1.1 Solar energy and solar cells

Eighty-seven percent of energy is produced from traditional resources including coal, nuclear, oil and gas, etc. [58] However, these energy sources will be depleted in the foreseeable future and can never be regenerated. In addition, the process of power production often pollutes the environment in terms of wasted water and gas. The gradual depletion of non-renewable resources leads to the deterioration of the environment. Therefore, development of an environmentally-friendly renewable energy resource is needed.

Solar energy is a promising renewable energy alternative for the fossil fuel energy; it will never be exhausted and the process of developing solar energy does not threaten environment. There are several ways of making use of solar energy, one being the converting solar energy to electricity by using a photovoltaic device. Presently, three kinds of photovoltaic devices are dominant: crystalline silicon solar cells, solar cells based on thin film polycrystalline semiconductor materials ($CuInSe_2$, CIGS and CdTe), and organic solar cells made from conjugated polymers, small molecules, dyes and inorganic-organic hybrids. [59]

3.1.2 Current density- voltage curves

Photovoltaic devices are characterized by current density-voltage (J-V) curves. A typical J-V curve is shown in the figure below. The parameters of short circuit current density (J_{sc}), open circuit voltage (V_{oc}), fill factor (FF) and power conversion efficiency (η) are all derived from J-V curves.

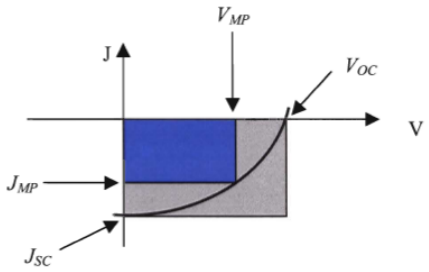

Figure 5. Typical *I-V* curves

3.1.3 Open circuit voltage and short circuit current

The short circuit current density (J_{sc}) and the open circuit voltage (V_{oc}) are two crucial characteristic parameters for solar cell performance. They can be measured in white light illumination process using a multimeter. The short circuit current (J_{sc}) can be measured when the device is working with zero resistance. The built-in potential produces the short circuit current by forcing the photogenerated charges to drift to electrodes when the device is working without external voltage. The open circuit voltage (V_{oc}) is the voltage when the device is connected to an infinite resistance load. If the external applied voltage is equal to the open circuit voltage, the short circuit current can be compensated to zero. Therefore, for J-V curves, the intersection of the curve and x-axis is referred as V_{oc} and the point where the curve and y-axis meets is J_{sc}.

3.1.4 Fill factor

Fill factor represents the quality of solar cell. It is defined as the ratio (given as percent) of the actual maximum obtainable power to the theoretical power.

$$FF = \frac{J_{MP}V_{MP}}{J_{SC}V_{OC}}$$

Where J_{MP} and V_{MP} represent the current density and voltage at the maximum power point, this point being obtained by varying the resistance in the circuit until $J \times V$ is at it's greatest value. When the solar cell with a higher fill factor is working under a maximum voltage, more electric power will be extracted at a constant current source. Theoretically, *FF* values are between 0.25 and 1, but it may drop below 0.25 at the presence of blocking contact at the electrodes.

3.1.5 Energy conversion efficiency

The energy conversion efficiency is the ratio between the maximum power output and the incident optical power input. It can be expressed in terms of J_{sc}, V_{oc} and *FF* as:

$$\eta = \frac{(FF)V_{oc}J_{SC}}{P_{light}}$$

3.2 Conductive polymers

3.2.1 Introduction to conductive polymers

Conductive polymers were developed as a novel class of photovoltaic materials with the potential of low cost, light weight and flexibility by Nobel Prize winner Alan J. Heeger, Alan G. MacDiarmid, and Hideki Shirakawa in Chemistry, 2000. [60]

Conjugated polymers are conductive because there are conjugated double bonds along the backbone of the polymer. There are alternating single and double bonds between the carbon atoms in this structure [60]. Every double bond also contains a localized "pi" (π) bond and a "sigma" (σ) bond. The sigma bond is a strong bond while the pi bond is a weaker bond. The existence of π-bonds makes these polymers have the semiconducting properties. First, the π-bonds are delocalized over the entire molecule; then the overlap of p_z orbitals actually produces two orbitals, a bonding (π) orbital and an antibonding (π^*) orbital. The lower energy π-orbital serves as the highest occupied molecular orbital (HOMO), while the higher energy π^*-orbital forms the lowest unoccupied molecular orbital (LUMO). The difference in energy between the two levels produces the band gap energy which is usually 1.5-3eV for most conjugated polymers. Therefore, an incident visible-light photon has sufficient energy to excite an electron from HOMO to LUMO in conjugated polymers. This property makes them suitable visible light absorbing photovoltaic devices.

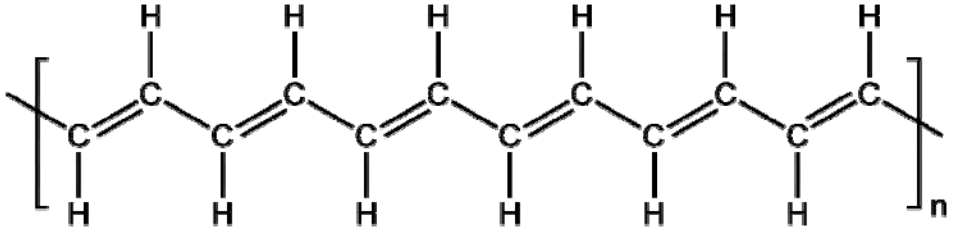

Figure 6. Atomic structure of oxyacetylene [56]

However, conjugation along is too weak to make the polymer material have the conductive behavior. Atoms with extra electrons or "holes" are added into the material via a doping process. It has been reported that oxidation with chlorine, bromine or iodine vapor can make polyacetylene thin film 10^9 times more conductive.[60] By analogy with the group III-V elements doping, treatment with halogens is called "doping". After the doping treatment, the polyacetylene had a conductivity of 10^5 Siemens per meter, which is the best polymer conductor [60]. Halogen doping transforms polyacetylene to a good conductor of electricity by oxidation (or *p*-type doping). Reductive doping (called *n*-doping) is also possible using, e.g., an alkali metal. The doped polymer is thus a salt.

$$[CH]_n + 3x/2I_2 \rightarrow [CH]_n^{x+} + xI_3^- \qquad \text{Oxidation doping}$$

$$[CH]_n + \text{xNa} \rightarrow [CH]_n^{x-} + \text{xNa}^+ \qquad \text{Reductive doping}$$

Conjugated polymers with alternating single and double bonds have been explored widely in photovoltaics, light-emitting diodes, photodetectors, transistors and sensors[61]. Polymer photovoltaic devices have recently attracted much attention and have shown great potential in the ongoing effort to lower the cost of solar cells. The conjugated polymers serve the function of electron donor material in organic solar cells. Most of these polymer materials are usually soluble in certain organic solvents. Therefore, through the inexpensive liquid based processing techniques such as spin coating,[62] doctor blading[63], ink jet printing etc., large area thin film solar cells can be manufactured. [64] The cost of making solar cells will be decreased and solar cells made from polymers are commonly light weight and flexible. The solvents typically used include toluene, chloroform, chlorobenzene, xylene, and dichloromethane. [58] However, all of those solvents are harmful to people and will pollute the environment, leading to the high cost,

complicated waste disposal processing. So it is helpful to develop an organic solar cell based on polymer which can dissolve in an environment-friendly liquid.

However, organic semiconductors have several disadvantages when employed in solar cells:

(1) Free charge carriers are not directly generated from the photo absorption process. Rather, electron-hole pairs referred to as "excitons" with typical binding energies of several hundred meV are formed. Excitons have to dissociate into charge carriers.

(2) The diffusion lengths of excitons and of free carriers are typically in the nm range. Photogenerated charge carriers have to be directly transported to electrodes or they will be lost by recombination.

3.2.2 Water-soluble conjugated polymer

Water-soluble conjugated polymers have a polar molecular structure, as does the water molecule. Therefore, this type of polymer can dissolve in the water. It has been reported that conjugated polymers with polar groups such as sodium poly (3-thiophene-β-ethanesulfonate) [P3-ETSNa], sodium poly(3-thiophene-δ-butanesulfonate) [P3-BTSNa] and their respective acids forms P3-ETSH and P3-BTSH serve as an alternative to the widely used solvent based polymers. [65] Recently, sodium poly [2-(3-thienyl)-ethoxy-4-butylsulfonate]) [PTEBSNa] and its acid PTEBSH have also been developed. In addition to the obvious environmental benefits, a water-based polymer solar cell has other advantages, one being its tuneability. It has been reported that acidic solutions of PTEBS develop a new absorption band in the near-IR and show increased absorption in the UV region [9]. The absorption spectrum of PTEBS polymer can be changed chemically; this

increased absorption also opens the possibility for building tandem junction cells with layers made using both acidic and basic solutions in order to match a greater portion of the solar spectrum.

Photogenerated excitons in polymer are strongly bound and resist dissociation into separate charges. Furthermore, these materials also have the disadvantages of low charge mobility and short exciton diffusion lengths. [66] Therefore, the performance of the solar cells made from homogenous polymer layers has been limited. The invention of heterojunction structure with phase separation between the polymer and certain inorganic nano-particles such as TiO_2 and CdSe have steadily increased the device efficiency over the last decade.[66] Poly (3-alkylthiophene (P3HT) is a conjugated polymer with good solubility and electron mobility; it has been integrated into hulk heterojunction solar cells To date, the highest reported power conversion efficiency for single junction solar cell is 5%, [67] under AM 1.5 illumination has been reported for P3HT bulk heterojunction solar cells.

3.3 Device concepts and architecture

3.3.1 Single layer devices

The single layer solar cell is the simplest design of polymer solar cells. A homogeneous layer of organic polymer is placed between two metal electrodes; as shown in Figure 7 below. This is also called metal-insulator-metal (MIM) structure. Conjugated polymers including polyacetylene, [68] polythiophene [69] and poly (para-pjenylenevinylene) (PPV) [70] have been used to fabricate solar cells in this structure. However, due to the inefficiency of photogenerated charge generation, the performance of the MIM devices is limited. It has been reported that the open circuit voltage is about 1.7 V and external energy conversion efficiency is less than 0.1% in ITO/PPV/Ca solar cells [45]. In photovoltaic applications, the electric field causes the separated photogenerated charges to be transported to the electrodes. However, the Coulomb force in conjugated polymer layer is strong enough to bind the photogenerated excitons. Marks *et al.* estimated the exciton binding energy approximately to be 0.4 eV in PPV. [70] The electric field generated by voltage difference between two electrodes is not high enough to dissociate the excitons into electrons and holes. In order to be dissociated, the excitons must diffuse to the organic-metal interface. However, since the exciton diffusion lengths for most conjugated polymers are between 5 nm and 15 nm, [71] most of the excitons will radiatively or non-radiatively decay before they actually reach the electrodes. This phenomenon limits the thickness of the device to the range of exciton diffusion lengths of conjugated polymer, making a great obstacle for device fabrication.

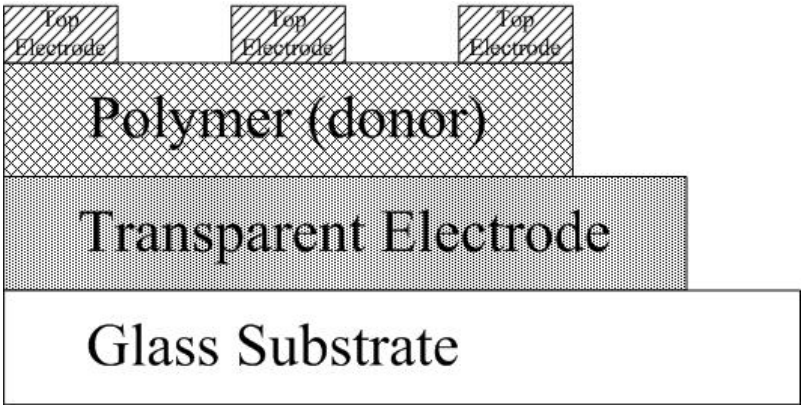

Figure 7. Schematic illustration of MIM structure device

3.3.2 Bilayer heterojunction devices

Bilayer heterojunction solar cells have been developed to improve the device photovoltaic device performance. As shown in Figure 8, this structure contains a separated interface between two different donor/acceptor materials in heterojunctions. If the potential energy between donor and acceptor material is larger than the exciton binding energy, the exciton will be dissociated and transferred to corresponding electrodes. Early efforts to develop organic heterojunction solar cells were based on the fabrication of an electron-transporting dye such as rhodamine and a hole-transporting dye such as phthalocyanine. [72] Tang was the first to make a bilayer heterojunction solar cell. [73] The device was made by evaporating a 50-nm thick perylenetetracarboxylic derivative (PV) layer on an indium tin oxide (ITO) glass. The energy conversion efficiency was 0.95%.

In polymer solar cells, *p*-type conjugated polymers such as MEH-PPV, [74] P3HT, [75] and PTEBS [39] have served as donors and inorganic semiconductors nanoparticles such as TiO_2, [71] CdSe, [76] carbon nanotubes[77] have served as acceptors. An incident

photon excites the electrons in the polymer and generates an exciton. The bound exciton then dissociated at the interface between the donor and acceptor material. This bilayer configuration thus generates the free charges and reduces the possibility of recombination of excitons.

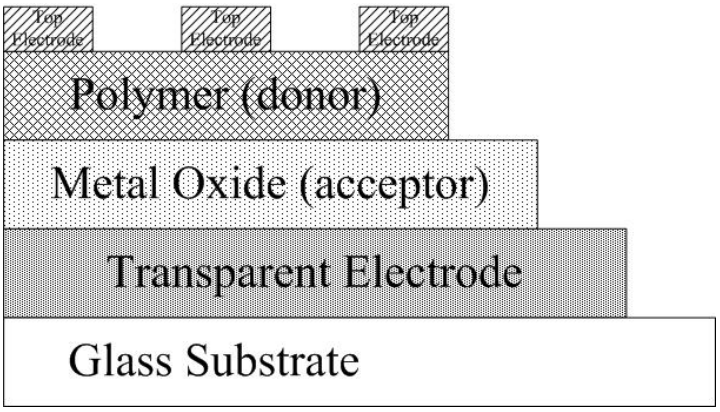

Figure 8. Schematic of illustration of Bilayer structure devices

3.4 PTEBS/Metal oxide bilayer solar cells

3.4.1 Bilayer/Bulk heterojunction PTEBS polymer/nanocrystalline TiO_2 solar cell

Bilayer and bulk heterojunction PTEBS/nanocrystalline TiO_2 photovoltaic devices have been designed and fabricated by Qiao et al. [58,64] The polymer was applied using a modified doctor blade technique. They used PTEBS as the electron donor and TiO_2 as the electron acceptor. The bilayer device configuration was glass/FTO (Fluorine doped Tin Oxide)/ TiO_2/PTEBS/Au and is shown in Figure 9:

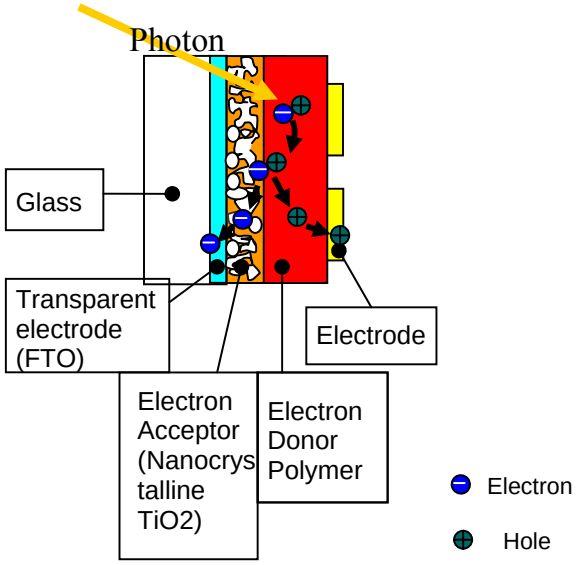

Figure 9. Schematic of Bilayer PTEBS/nanocrystalline TiO_2 heterojunction solar cell

In a bilayer heterojunction, an inorganic semiconductor TiO_2 is deposited onto a SnO_2 transparent electrode, as shown in Figure 9. The polymer is then spin-coated or dip-coated on top of the semiconductor. The device showed significant photovoltaic behavior with an open circuit voltage of 0.81 V, a short circuit current density of 0.35 mA/cm^2, and a fill factor of 0.4. This study showed that the polymer provides significant

photovoltaic response and has the potential to be used as electron donor in solar cells replacing solvent-based polymers. The power conversion efficiency of 0.13% has been achieved. [64]

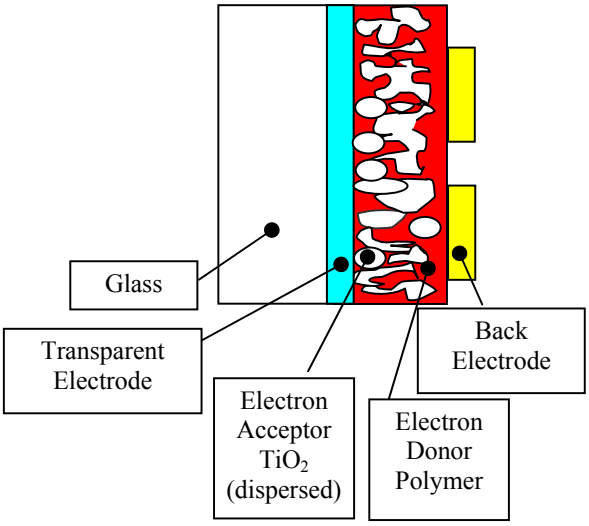

Figure 10. Schematic of Bulk PTEBS/nanocrystalline TiO_2 heterojunction solar cell

In a bulk heterojunction, nanocrystalline TiO_2 and PTEBS polymer are mixed together creating a heterogeneous composite with a high interfacial surface area, as shown in Figure 10. Since the charge separation tends to occur at the interface between semiconductor and polymer, this enhances the charge separation rate therefore create more charge carriers. The devices achieve an energy conversion efficiency of 0.056%, a short circuit current of J_{SC}=0.16 mA/cm^2, and open circuit voltage of V_{OC}=0.85 V [58].

Although the organic solar cells made from TiO_2 nanocrystalline/PTEBS showed photovoltaic behavior, the problems of bilayer solar cell mentioned in 3.2.1 still existed in the bilayer devices. In a TiO_2 bilayer device, the TiO_2 nanoparticles bind to each other and form a direct path to the electrode. However, the interfacial area between the polymer and the TiO_2 is limited; therefore there is limited exciton separation. For the bulk heterojunction devices, TiO_2 nanoparticles served as electron acceptor, the electrons must

travel between isolated nanoparticle to the collecting electrode. Obviously, a direct path is not formed, which result in the exciton recombination.

3.4.2 Hybrid PTEBS polymer/ZnO nanowires solar cell

In order to decrease the possibility of excitonic recombination thereby increase charge transport efficiency, a direct and ordered path for electrons to the collecting electrode should be applied into solar cell. In addition, the device should also have large interface between the polymer and the electron acceptor. The application of semiconductor nanowires within devices is one of the major focuses of contemporary nanotechnology. ZnO has great potential to be useful in nanostructure photonic devices. [5] The use of ZnO nanowires in polymer based heterojunction solar cells would have several advantages as compared to existing nanoparticle based solar cells.

First of all, ZnO nanowires can improve exciton separation by reducing distance the exciton must travel to the interface. The ZnO nanowires will then provide a direct path for photogenerated electron traveling through to the collecting electrode thereby decrease the possibility of the recombination.

Secondly, the ZnO nanowires have certain length; it allows a thicker polymer layer surrounding them, which will lead to more solar light absorption.

Thirdly, it is well known that the properties of nanostructure materials depend on their crystal size, morphology, aspect ratio and orientation. Single crystalline ZnO nanowires show mobility as high as 80 cm^2/Vs [29]. And Park *et al.* have reported an electron mobility of 1000cm^2/Vs [30] after coating the nanowires with polyimide to reduce the electron scattering and trapping at surface. These results indicate that using designed ZnO nanowires, one can tune the carrier concentration and mobility of the nanowire,

providing a way to modify the electrical properties and thereby improve the transport of electrons to collecting electrode.

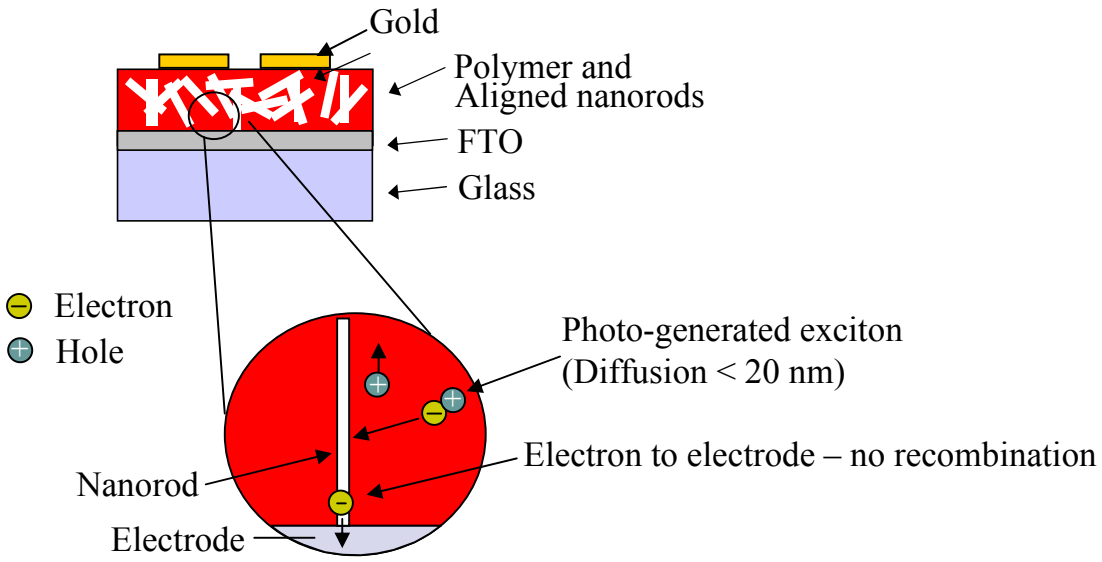

Figure 11. Zinc oxide nanowires in solar cells

The figure above illustrates the functionality of zinc oxide nanowires in organic solar cell. The nanowires are grown from the substrate, therefore photogenerated electrons travel directly through the nanowire to the transparent electrode. It has been reported that excitons separate into holes and electrons at the polymer-ZnO nanowire interface. Since the surface-to-volume of nanowires is high, the ZnO nanowires enhance the exciton separation therefore improve the charge separation. In addition, electrons are able to travel through the nanowires without recombining with holes. It can thus improve the charge transport in solar cell.

Recently, Peiro *et al*. [5] reported the use of ZnO nanorods in hybrid polymer/zinc oxide (ZnO) solar cells, in which the metal oxide consists of ZnO columnar structure grown perpendicularly on a ZnO seed layer. The vertically aligned ZnO columnar layer served as a direct and ordered path for photogenerated electrons to the collecting

electrodes. Fig. 12b and c [5] show the two active layer designs that have been investigated in this work, namely a backing layer in contact with a polymer film and a columnar structure grown on top of a backing layer, with the polymer interpenetrating the structure.

The ZnO backing layer was deposited onto ITO substrates through several chemical methods, including dip-coating, spin-coating, and spray-pyrolysis [5]. Different ZnO precursor concentrations and spin velocities were evaluated in spin-coating method. However, pinholes were present in these films that could be seen with the naked eye, indicating poor film quality. For the spray-pyrolysis method, zinc acetate was dissolved in methanol as precursors; transparent films were obtained with DMF (dimethylformamide) in the solution. Then, ZnO columnar structures were prepared on the three different backing layers: (1) Dip-coated porous ZnO layers, (2) Spray-Pyrolysis compact ZnO layers and (3) Spray-Pyrolysis compact TiO_2 layers.

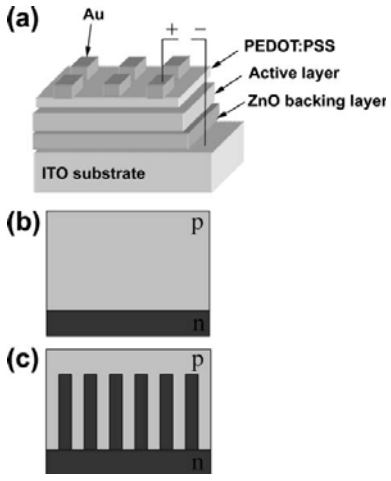

Figure 12. Configuration of hybrid polymer/ZnO nanowire solar cell (a) Schematic of the device structure studies in this work. (b) Backing layer in contact with a polymer film (bi-layer structure) and (c) Columnar structure grown on top of a backing layer, where the polymer is interpenetrating the surface. [5]

The growth of vertically aligned ZnO nanorods and nanowires was performed in aqueous solutions. The ZnO nanowire grown on spray-pyrolysis ZnO backing layer had an average diameter of 100 nm and length of 730 nm, which fits the requirement of fabrication of organic solar cells. Different conjugated polymers (MEH-PPV and P3HT) have been utilized in organic solar cells in this work.

After recording the data from different experiments, the best result was obtained based on the Spray-Pyrolysis ZnO backing layers with P3HT polymer (power conversion efficiency η=0.20%)

Chapter 4 Experimental Section

4.1 Controlled growth of Zinc Oxide nanowires

4.1.1 Nanowires synthesized via chemical vapor deposition method

4.1.1.1 Equipment and material

(1) Atomate low-temperature Chemical Vapor Deposition system

The low-temperature Chemical Vapor Deposition system was built by Atomate Corporation. It includes a Mini-Mite^{TM} horizontal tube furnace heating element with leak-proof sealing, a rotary pump system, a MKS^{TM} Baratron type 722A pressure transducer, a MKS^{TM} type 146C gauge vacuum gauge measurement and gas flow control system.

The Mini-Mite^{TM} tube furnaces are ultra lightweight, economical laboratory tube furnaces. The dimension of the tube furnace is 2.5×30.5 cm. It provides fast duty cycles, energy conservation, and efficient programming. The furnace is equipped with a UP 150 temperature controller, which senses the chamber air temperature of the furnace, and supplies the heat necessary to achieve the desired setpoint. With the controlled heat-up rate, it eliminates thermal shock to materials. The unit is rated for a maximum operating temperature of 1100 ^{o}C. In addition, digital instrumentation enables the precise temperature setpoint and display, the microprocessor in UP 150 controller automatically optimizes control parameters during furnace operation.

The pressure inside of furnace tube is controlled and monitored by MKS Baratron Type 722A Absolute Pressure Transducer. The 722 transducer contains the sensor and signal conditioning electronics. The sensor is connected to a small chamber in the transducer body; one wall of this chamber is a metal diaphragm. The front side of the diaphragm is exposed to the gas whose pressure is to be measured. The back side faces a rigidly mounted ceramic disc containing two electrodes. Signal conditioning electronics contain balance bridge circuitry, self- compensated for thermal stability with ambient temperature changes.

The carrier gas flow rate is controlled by MKS Type 146C Cluster Flow Controller equipped with a Vacuum Gauge Control System. It powers and provides simultaneous readout for four different vacuum gauges or mass flow controllers. Two dual-channel features are provided to automatically switch from one gauge to another allowing continuous pressure display. There is an automatic ion gauge power down at high pressures and a sensor power down for cryopump regeneration.

The chemical vapor deposition system used for nanowire synthesis has a precise computer control over the growth variables including: growth time, reaction temperature and carrier gas flow rate. The Atomate Workbench software has been installed along with a graphical user interface. It enables efficient controls over the mass flow controllers and quartz tube furnace through a multiple user password protected log-in, automatically storing process recipes and run data, and improving process control with conditional modifiers for each step of the process.

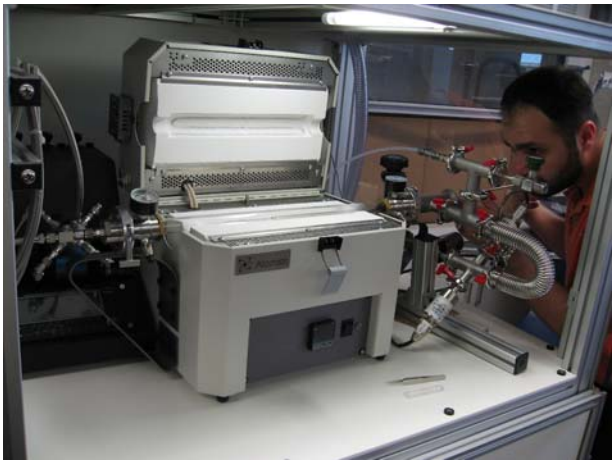

Figure 13. Atomate low-temperature chemical vapor deposition system

(2) Ernest Fullam sputtering coating facility

A thin gold thin film was deposited on the FTO substrate in advance via sputter coating process. The sputter coating device is a compact coater intended for coating non-conductive specimens. When a target is bombarded with fast heavy particles, erosion of the target material occurs, this is termed sputtering. This process occurs in the conditions of a gaseous glow discharge between an anode and cathode. Some of the sputtered atoms will condense on the surface of the specimen to be coated, forms a thin gold film.

The sputter coating machine used in this thesis was fabricated by Ernest Fullam Inc. As shown is Figure 14. Samples can be coated in less than 30 seconds with high-rate target, as shown in Figure 15. The table below is the specification of Ernest Fullam sputter coater.

Table 2. Specification of Ernest Fullam sputter coater

Input power	115V AC, 60 Hz, 200 watts
Weight	22lbs
Dimensions	10.5”W×13”H×10”D

Chamber size	4" dia × 3"H
Operating Vacuum	200-300 mm Hg
Operating Current	Up to 200 milliamps-High Rate
Pumping Time	20-60 seconds

The thickness of the gold film is dependant on the deposition time (see section 5.1). The effect of the thickness of gold thin film upon the size of catalyst droplet in VLS process has been investigated.

Figure 14. Sputter Coating Facility

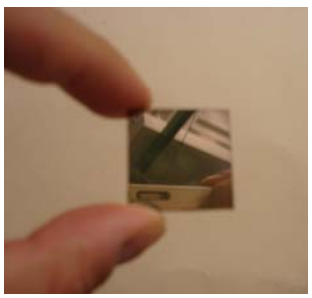

Figure 15. FTO substrate coated with gold thin film

(3) Scanning electron microscope

The morphology of the samples was studied using an EVO MA 15 Scanning electron microscope (SEM) provided by Zeiss Inc. With a motorized 5 axis stage with

large XY and Z travels (Motorized Z movement of 50 mm, X and Y both 125 mm); variable pressure capability and easy to use SmartSEM software, the EVO MA 15 offers an imaging solution in fields from geology, forensics, and failure analysis. The EVO MA 15 delivers great clarity of the finest structure; the highest resolution is 3.0 nm at 30 KV. In addition to the high resolution at several hundreds of times greater than that of the optical microscope, the focal depth of SEM imaging is several tens of times greater than the optical microscope. Therefore, the SEM allows for detailed measurements, including 3D measurement from stereo images. Several other features have also been developed in this serial including: Remote diagnostics over the internet, improved low KV imaging, and largest specimen height increased to 145 mm. The figure below listed the specifications of EVO MA 15 SEM.

Table 3 Specification of EVO MA 15 scanning electron microscope

Resolution	3 nm (2 nm) @ 30 kV 20 nm (15 nm) @ 1 kV 10 nm @ 3 kV
Acceleration Voltage	0.2 – 3.0 kV
Magnification	<5 – 1,000,000 x
Field of view	6 mm at the Analytical Working Distance (AWD)
Pressure Range	10 – 400 Pa
Chamber	365 mm (Φ)×275 mm (h)
5-Axes Motorized Specimen Stage	X shift : 125mm Y shift : 125mm Z shift : 50 mm

	Sample Tilt : 0-9^{o} Sample Rotary : 360^{o} (continuous) Stage control by mouse or optional joystick and control panel
Maximum Specimen Height	145 mm
System Control	Smart SEM; Windows XP multilingual operating system

Energy dispersive spectroscopy (EDX) has been utilized to analyze the chemical composition of as-synthesized nanostructure. Usually, the EDX systems are most commonly found on scanning electron microscopes (SEM-EDX). A DS-130 Dual Stage Scanning Electron Microscope is utilized for imaging and energy dispersive X-ray analysis in this work. This instrument is provided by ABT company, has the capability to do SEM, STEM (scanning transmission electron microscopy) and EDX analysis.

In this SEM system, top stage is designed for SEM imaging while EDX measurement was carried out at lower stage. For SEM imaging process, the specimen is placed between the objective lens and collects the imaging electrons above the lens. The high electron efficiency provides a resolution of 3nm with ideal samples. The lower stage allows specimens up to 10cm diameter to be examined with a resolution of 6nm. Both stages are fitted with EDX Si/Li detectors. The figure below is the specifications of this SEM system.

Table 4 Specification of ABT DS-130 dual stage scanning electron microscope

Resolution	4 nm @ 30 kV, Secondary electron image
Acceleration Voltage	0.5 to 3.0 kV (100V steps), 3 to 30kV (1kV steps)
Magnification	<5 – 1,000,000 x
Lens system	3-step lens system (2 condenser lenses, and 1 object len)

Image modes	Secondary electron image; Backscattered electron image
Chamber	780mm (Φ)×1,340mm (H) ×600(W)
Motorized X-Y Specimen Stage	X shift: 80mm Y shift: 60mm Z shift: 50 mm Specimen Tilt: -10^{o} to 90^{o} Specimen Rotary: 360^{o} (continuous) X and Y movement driven by motor with joystick control
Maximum Specimen Size	150 mm diameter. (Lower stage); 50 mm diameter. (Upper stage)
System Control	Computer-controlled auto focus system; Windows XP multilingual operating system

(4) Chemicals and substrates

Zinc oxide nanopowder and graphite powder were utilized as precursor material. Zinc oxide nanopowder of 99.999% purity was provided by Aldrich Corporation and graphite powder of 99.9995% purity was provided by Alfa Aesar Corporation.

Fluorine-doped tin oxide (FTO) substrates are glass squares coated with SnO_2 thin films, and are widely applied in fabricating organic solar cells. In this work, FTO coated glass squares (2.5cm × 2.5cm) were used as the substrate in the CVD system and as the bottom electrode for solar cell fabrication. The FTO coated glass was purchased from Hartford Glass Co. Inc. and has a resistance of 12.5-14.5 ohms/square and layer thickness of 400nm.

4.1.1.2 Experimental procedure

A modified CVD synthesis method with a vapor trapping design has been carried out. A quartz inlet tube (Inner diameter: 8 mm; Outer diameter: 10 mm; Length: 23 cm) placed in the furnace tube was used to maintain high zinc vapor concentration around the growth environment. The furnace tube was evacuated before the experiments; therefore, the oxygen content is dilute. The rate of zinc vapor diffusing from the inlet tube was relatively low since growth was conducted at 1 atm. In this unique mechanism, a zinc vapor concentration decreases from inside to outside of inlet tube, therefore, a high zinc concentration environment has been maintained in the inlet tube. The Figure 16 below illustrates this experiment setup.

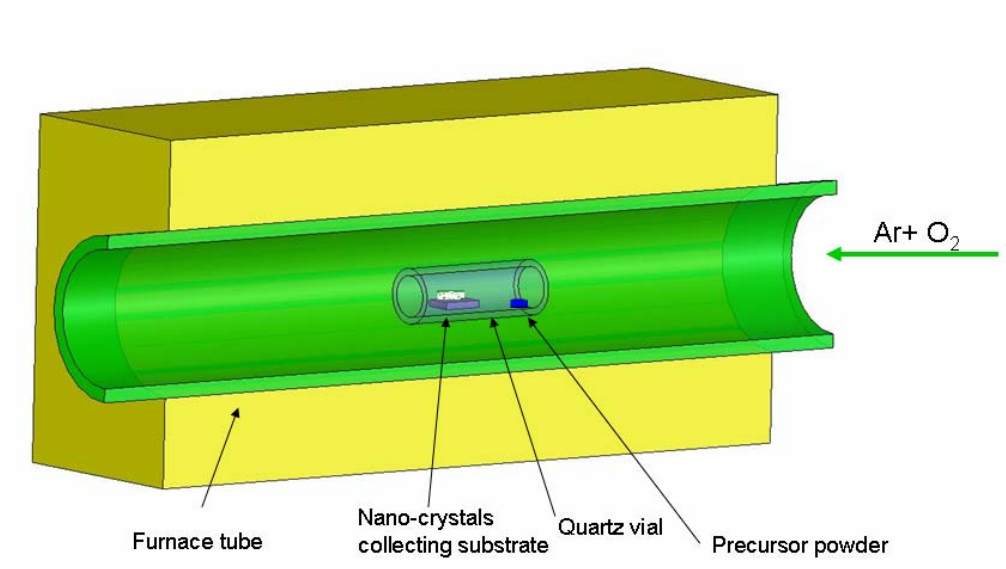

Figure 16. Schematic illustration of chemical vapor deposition system with an inlet quartz vial tube place inside of tube furnace.

Clean FTO coated glass samples were prepared as substrates in the CVD system. Due to the size limitation of the inlet tube, 2.5 cm × 2.5cm square FTO coated glass substrates were sliced into small pieces (usually 5 mm × 5 mm) for the CVD system. The

substrates were sputter-coated with thin gold film. A mixture of ZnO and graphite powder in a certain weight ratio (1:1 ZnO/graphite) was placed upstream inside of the inlet quartz tube and served as precursor while substrates placed at the other side of the inlet tube. The synthesis experiments were carried out in the following steps:

1. Check the fume-hood and make sure it is operational. The exhaust tube at the top of the instrument's upper cabinet should be tightly connected to the fume-hood to ensure the waste gas is not leaking to the atmosphere.
2. Check the Argon gas cylinder. The gauge should show at least ¼ full.
3. The precursor is mixed zinc oxide and graphite powder at a weight ratio of 1:1. Weight out 60 mg of the precursor using the analytical balance and place close to the left side of the quartz inlet tube.
4. Pick the desired substrates (glass or silicon) and place about 4 cm away from the precursor to the right of the quartz inlet tube.
5. Place the inlet quartz tube inside of the quartz furnace tube. The right end of quartz inlet tube should be 15mm away from the right edge of furnace tube. The inlet tube should be placed as shown in Figure 17.

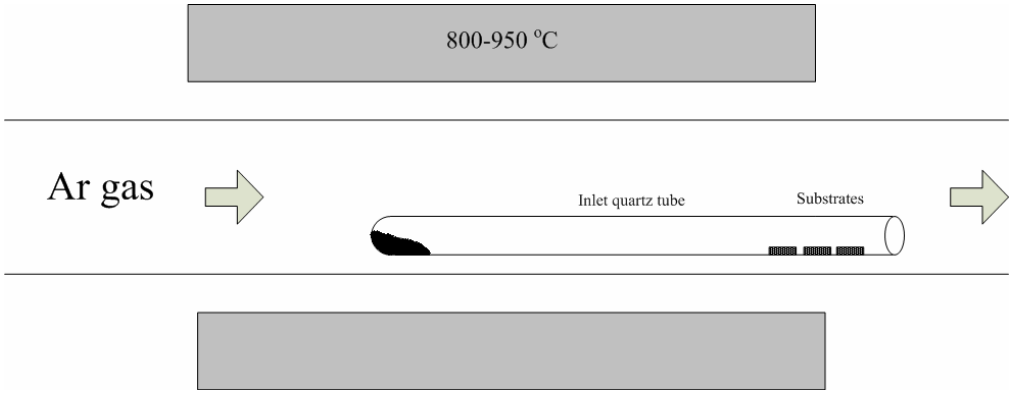

Figure 17. Experimental setup of vapor trapping CVD mechanism

6. Use the hand pump to regulate pressure around quartz furnace tube's O-rings (~70 kPa).
7. Turn on the computer and enter the user id and password.
8. Turn on the furnace and gas flow controller. Open the gas tank valves; make sure the bypass valve and the green valve, which is connected to the atmosphere, are securely closed.
9. Turn on the vacuum pump located on the right side of the lower cabinet and wait for 3 minutes to warm up.
10. Evacuate the chamber by slowly opening the bypass valve. It is very important to do this very gradually to prevent the precursor from getting evacuated as well. If this occurs the system must be broken down for cleaning. Close the valve securely after the chamber gets evacuated.
11. Adjust the recipe controls using the Atomate software according to specific growth time, furnace temperature and gas flow rate of the experiment been carried out.
12. After adjusting the controls to desired values, start the run by clicking on the green "play" icon. At that specific moment, carrier gas should flow in the tube and pressure should adjust quickly to the set value.
13. The first few minutes of the run are very important, the gas regulator, furnace, and pressure controller should be checked simultaneously during the time of operation. The system should be following the software's recipe with minimum error margin.
14. After the temperature ramps down to about 200^{o}C, close the gas inlet and stop the run.

15. Gradually open the bypass valve to evacuate the chamber, and then open the green valve to regulate the pressure to 760 torr, which is atmosphere pressure.
16. Turn off the pump. It is important that the green valve is open before the pump been turned off.
17. Extract sample and place in appropriate sample container.
18. Label and date sample container.
19. Close gas tank and valves then clamp the vacuum flanges on the low pressure side to seal the system back up.
20. Place sample in clean room and dispose left over precursor in appreciate waste disposal bottle.
21. Clean quartz boat with distilled water and acetone. Dry and put back in clean room.

4.1.2 Seed layer controlled synthesis of well-aligned ZnO nanowire

4.1.2.1 Solution-growth of zinc oxide nanowires

Solution growth of zinc oxide nanowires is another approach for nanowire synthesis. The hydrothermal solution approach has many merits that can make ZnO nanowires grow at low temperature (<350^{o}C) at low cost. Two hydrothermal methods were investigated in order to prepare ZnO nanowire on substrate coated with ZnO dense layer [5,78].

Method 1 (*$ZnSO_4$/ NH_4Cl method*). An aqueous solution of zinc sulfate ($ZnSO_4 \cdot 7H_2O$, 0.02 mol dm^{-3}) and ammonium chloride (NH_4Cl, 0.6 mol dm^{-3}) was prepared. This solution was further diluted to 0.01 mol dm^{-3} in Zn^{2+} and then, the pH was

adjusted to 11.00 with sodium hydroxide (NaOH). Substrates with ZnO dense layers (see section 4.1.2.2) were immersed in this solution and ZnO nanowire deposition took place at 60^{o}C for 3-12 hours. Following deposition, substrates were sonicated in distilled water, and dried under nitrogen gas.

Method 2 (The hydrolysis of zinc nitride $Zn(NO_3)_2{\cdot}6H_2O/NH_4OH$ method). 0.025M of zinc nitrate hexahydrate ($Zn(NO_3)_2{\cdot}6H_2O$) was dissolved in deionized water. Then, 0.025M of hexamethylenetetramine (HMTA) was added to the solution. FTO substrate deposited with ZnO dense layer (see section 4.1.2.2) was immersed in this solution by suspending the wafer upside down in the solution. The growth process was carried out in an open bath 90^{o}C for 6 hours, the pH was adjusted to 7~9 with sodium hydroxide (NaOH). In this case, HMTA was decomposing slowly to provide a gradual supply of ammonia, which can form ammonium hydroxide (NH_4OH) to further adjust the pH value. Then the sample was removed from the solution after the growth process, sonicated with deionized water, and dried under nitrogen gas.

4.1.2.2 Zinc oxide seed layer preparation

In this work, a thin ZnO seed-layer coated with dense ZnO nanocrystals was introduced to control the density and orientation of ZnO nanowires. Spin-coating and dip-coating methods have been used to prepare the ZnO dense layer. [79,80] 99% purity zinc acetate was purchased from Fisher Scientific Inc. 99.5% pure ammonium chloride; zinc chloride; methanol and ethanol were purchased from Sigma-Aldrich Inc.

1) A 0.20 mol dm^{-3} solution of zinc acetate dihydrate in methanol. All the solutions were stirred overnight at room temperature, then spin-coated at 3000 rpm for 30s

onto the FTO substrate. The as-obtained films were dried at 70^{o}C for 10 min and calcined at 450^{o}C for 20 min.

2) A FTO substrate was wet with a droplet of 0.6 mol dm^{-3} solution of zinc acetate dihydrate in ethanol, rinsed with clean ethanol after 10 s, and then blown dry with argon gas flow. This coating step was repeated for three to five times. Then the sample covered with a film of crystalline zinc acetate, is annealed in a furnace at 350^{o}C for 20 min to decompose zinc acetate, forming zinc oxide islands. The zinc acetate deposition and decomposition procedure is carried out twice to ensure a complete and uniform coverage of ZnO seeds.

4.2 Design and fabrication of solar cell

4.2.1 Device fabrication

Hybrid zinc oxide nanowire/ PTEBS polymer solar cells have been fabricated in this study. The device architecture is shown in section 3.4.2. Due to the size limitations of CVD instrument and the inlet tube, a 2.5×2.5 cm square FTO glass substrate was sliced into small pieces for CVD experiments. The polymer layer was then deposited on the previously grown zinc oxide nanowires. The PTEBS polymer was dissolved in deionized (DI) water to a concentration of 1 %. A few drops of dimethyformamide (DMF) were added in the solution to enhance dissolution. The solution was stirred for at least two days and then left for 24 hours to settle the undissolved particles.

The PTEBS polymer was purchased from American Dye Source. A modified drop-casting technique was employed for polymer coating due to the low viscosity of the PTEBS water solution. As shown in Figure 18, a string frame was placed on the FTO substrate. The FTO substrate deposited with ZnO nanowires grown on top was placed on a 50^{o}C heating plate. A droplet of polymer water solution was dropped into the frame of the substrate. The thickness of deposited PTEBS film is controlled by the diameter of the strings; makes the PTEBS thickness quite homogeneous after layer-by-layer deposition. The film appears red color after the deposition and turns to auburn color when it is dry.

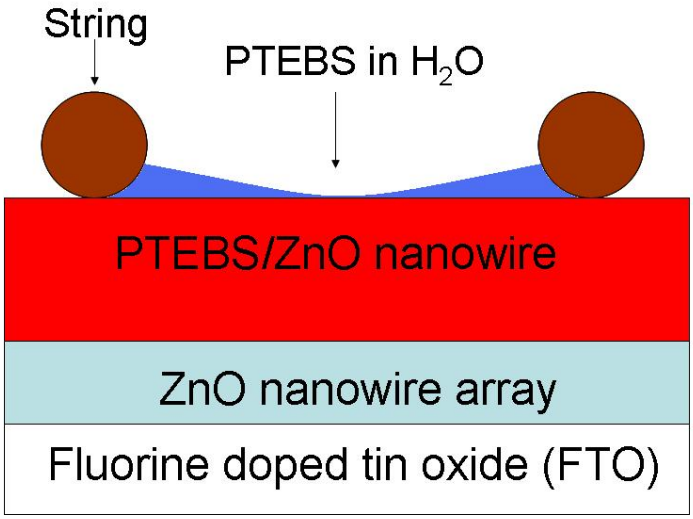

Figure 18. String frame setup for PTEBS/ZnO nanowire film deposition

Figure 19. FTO substrates: left to right: (1) FTO square (2) Coated with PTEBS polymer (3) Sputter coated with gold electrodes

In addition, PEDOT: PSS polymer was spin-coated on the device surface to improve the hole conductivity while blocking electron transport. Finally, gold electrodes were sputter-coated on to the polymer to make electrodes. Usually, mask was used to define the electrode area around 5×3 mm^2. The architecture of the zinc oxide nanowire/PTEBS polymer solar cell is shown in Figure20. Basically, the device consists of two electrodes (FTO and Au). Zinc oxide nanowires and PTEBS polymer layers lie in between. Photo-generated electrons move to the FTO through a hole-blocking layer (zinc oxide dense layer) and holes move to the Au electrode through an electron blocking layer (PEDOT : PSS polymer layer).

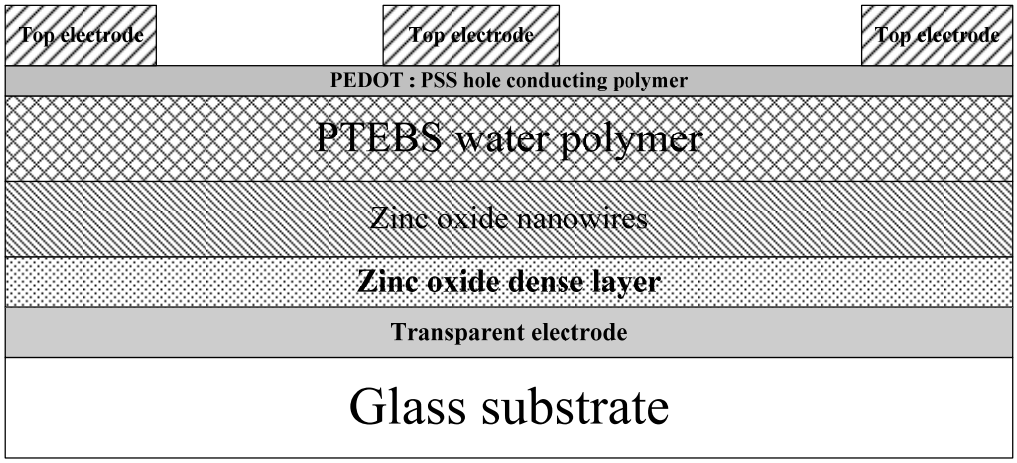

Figure 20. **Architecture of zinc oxide nanowire/PTEBS bilayer solar cell**

4.2.2 Current density- voltage measurement of solar cell

Solar cells are photodiodes and are generally characterized using current density-voltage (J-V) curves. The devices were tested in the dark and under AM1.5 illumination with an intensity of approximately 80 mW/cm^2 using a Keithley 236 source generator by varying the voltage from -3 V to 3 V in 0.04 V steps across the FTO and gold electrodes. The Figure 21 below is the I-V measurement system.

Figure 21. Current density-voltage measure system left to right (1) Keithley 236 source measure unit (2) Air Mass 1.5 illumination from Spectra-Physics Inc. (3) Tunable holding and testing instrument for solar cell *I-V* measurement.

A solar cell was placed in the testing instrument. The tip of the instrument was contact to each gold electrode while the SnO_2 electrode was connected to the Keithley 236 measure unit. Therefore, a circuit loop has been created. When a light beam from

illumination light shone on each of the electrodes, the photo-generated current and voltage data will then be accumulated and analyzed by the measure unit. *I-V* diagram was automatically generated by software written in LabView, which indicates the Open Circuit Voltage and Short Circuit Current. The fill factor and energy conversion efficiency of the device can be calculated from those data.

Chapter 5 Results and discussion

5.1 Investigation of gold catalyst particle morphology

To provide a catalyst layer for ZnO nanowire growth, thin gold films were sputter coated onto the FTO substrates, with deposition times of 10s, 20s, and 30s respectively. The thickness of the gold film on the FTO substrates were measured using a profilometer. The profilometer data in table 5 reveals the thickness of gold thin films as a function of sputter-coated in different time.

Table 5. The dependence of gold catalyst droplet diameter on sputter-coating time

Time (s)	10	20	30	40
Film thickness (nm)	9~13	19~24	27~35	41~46

After sputter coating, the substrates were heated in furnace at 950^{o}C for 100 minutes. The gold thin film melted into separate particles on the substrate surface as shown in Figures 22-24. SEM data have been collected to investigate the size of the particles deposited at different deposition time.

As the sputter-coating time increases, the gold droplets expand their sizes. For 10 seconds deposition, the average diameter was around 100 nm (Fig. 22).

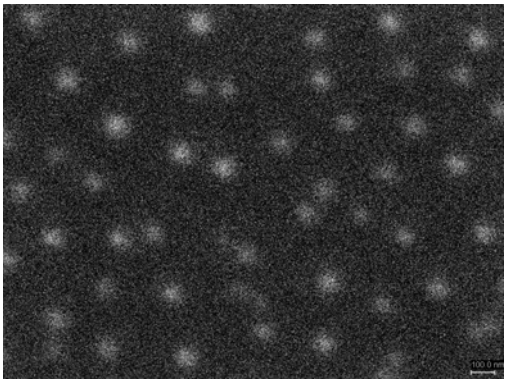

Figure 22. Gold droplets formed after 10 sec deposition have average diameter of 100 nm; Scale bar: 100 nm

For 20 second deposition, the average diameter has increased to about 150 nm (Fig.23).

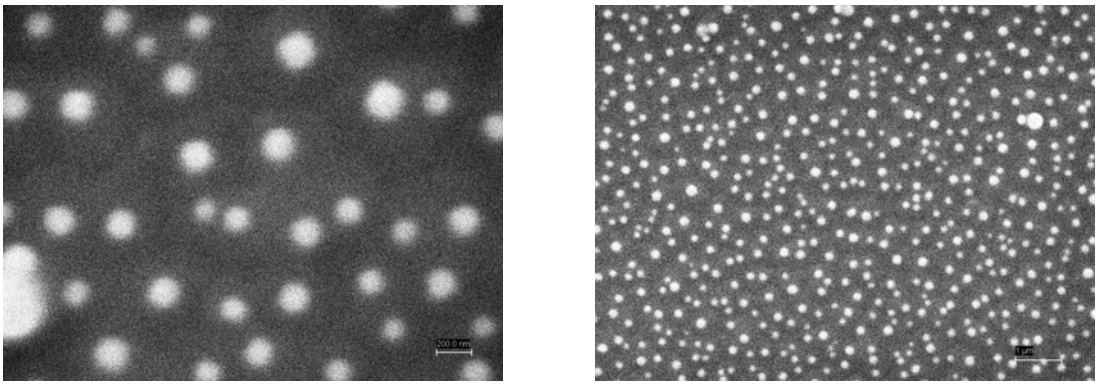

Figure 23. (a) Gold droplets formed after 20 sec deposition have average diameter of 150 nm; Scale bar: 200 nm. (b) The gold droplets were evenly distributed; Scale bar: 1 µm

When sputter-coated for 30 seconds, the average diameter has reached to 200 ~310 nm, while the number density of gold droplets is also increased

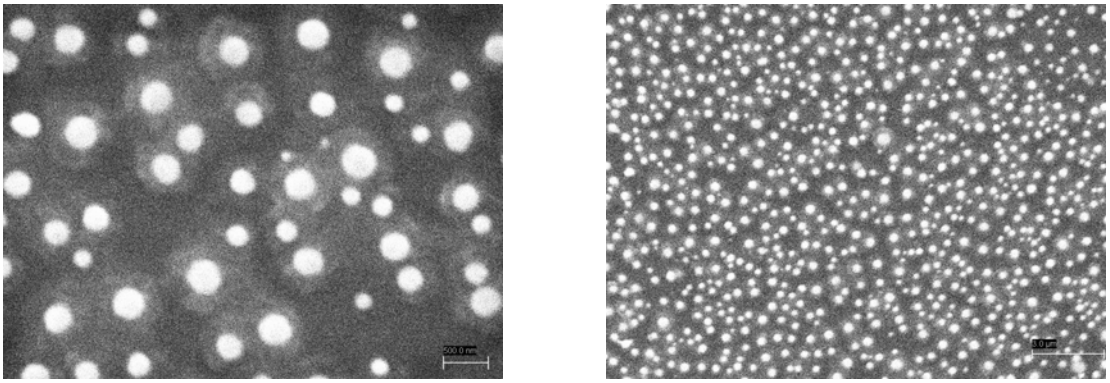

Figure 24. (a) Gold droplets formed after 30 sec deposition have average diameter of 200-310 nm**;** Scale bar: 500 nm. (b) The gold droplets were even more densely distributed; Scale bar: 5 μm

The droplets were evenly distributed on the substrate with uniform size, as shown in Figure 25. Basically, the size of gold droplets is proportional to the thickness of the sputter-coated gold thin film.

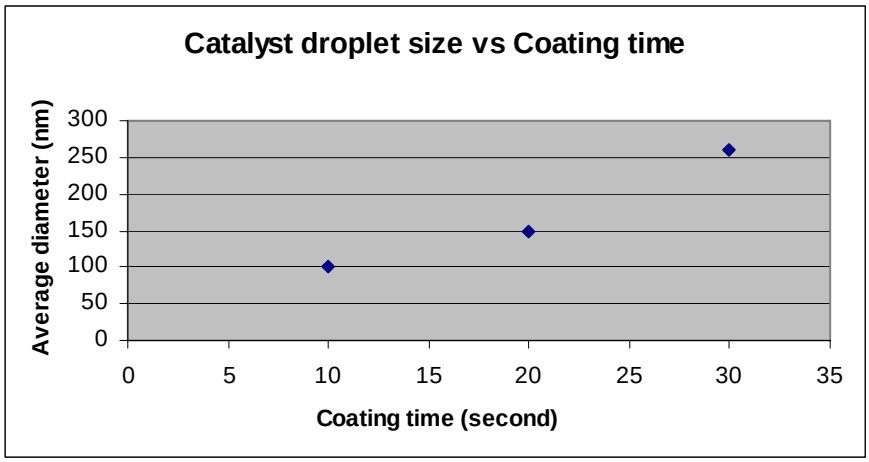

Figure 25. The dependence of gold catalyst droplet diameter on coating time

5.2 Variation of zinc oxide nanowires in chemical vapor deposition reaction

A parametric study of the effects of temperature, time, and gas flow rate on the length and the diameter of the ZnO nanowires has been conducted. Since the ZnO nanowires are produced for conducting layer in an organic hybrid solar cell, in order to maintain efficient charge separation in nanowire-based architecture, the nanowires must be thin (~50nm) and closely spaced, with a wire-to-wire distance equal to approximately twice the diffusion length of excitons in the polymer. Therefore, the average space between each single nanowire should equal or approach twice the maximum exciton diffusion length which is approximately $2 \times 20 = 40$ nm. [81] The goal of these experiments is to determine an optimized combination of these three controllable parameters which results in ZnO nanowires with desired morphology and density. The experiments were carried out with two parameters fixed while the third one was changing.

5.2.1 Effect of reaction time of as-synthesized nanowire morphology

The first group of experiments was carried out at 950^{o}C under the Ar flow rate of 70sccm; the reaction times were 30, 80, 100, and 120 minutes respectively. Figures 26 to 30 are the SEM images taken from each of these experiments, which revealed the effect of reaction time on the average diameter and length of as-synthesized ZnO nanowires.

5.2.1.1 Effect of Reaction time on Length

Figure 26 is a group of SEM images of the as-synthesized nanostructures on FTO glass substrate after 30 min of deposition at furnace temperature of 950^{o}C under Ar gas flow rate of 70 sccm. This characterizes the initial growth of ZnO nanowires.

Dispersively distributed ZnO nanoparticles with the dimension ranging from 100 to 150 nanometers in diameter were formed on the gold-coated FTO glass substrate. These nanoparticles served as seed layer for growth of ZnO nanowires, and as the reaction time increase, the nanowires grew outwardly from each nanoparticle site.

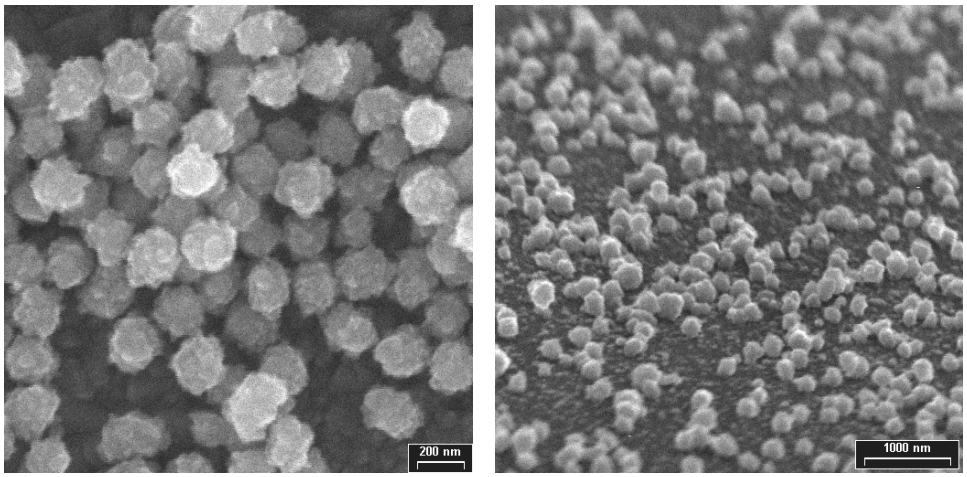

Figure 26. Initial growth of ZnO nanowire at FTO glass substrate with a growth time of 30 min. (a) ZnO nanocrystalline particles have just nucleated and start to grow. (b) Side view of the nanocrystalline particles showing their uniform shape and size.

When the growth time rose to 80 min with the argon flow rate and furnace temperature unchanged, the white wax-like materials appeared on substrate surface. The deposited products were characterized by scanning electron microscopy (SEM); it is shown in Figure 27 (a) that a high density of ZnO nanowires was grown from the nanoparticles. In contrast with the synthesized nanoparticles, the nanowires were distributed uniformly all over the sample. Figure 27 (b) and (c) are higher-magnification pictures which clearly illustrate the uniform size of the ZnO nanowires. The nanowires have the dimensions of 30 to 40 nanometers in diameter and 1 to 2 microns in length.

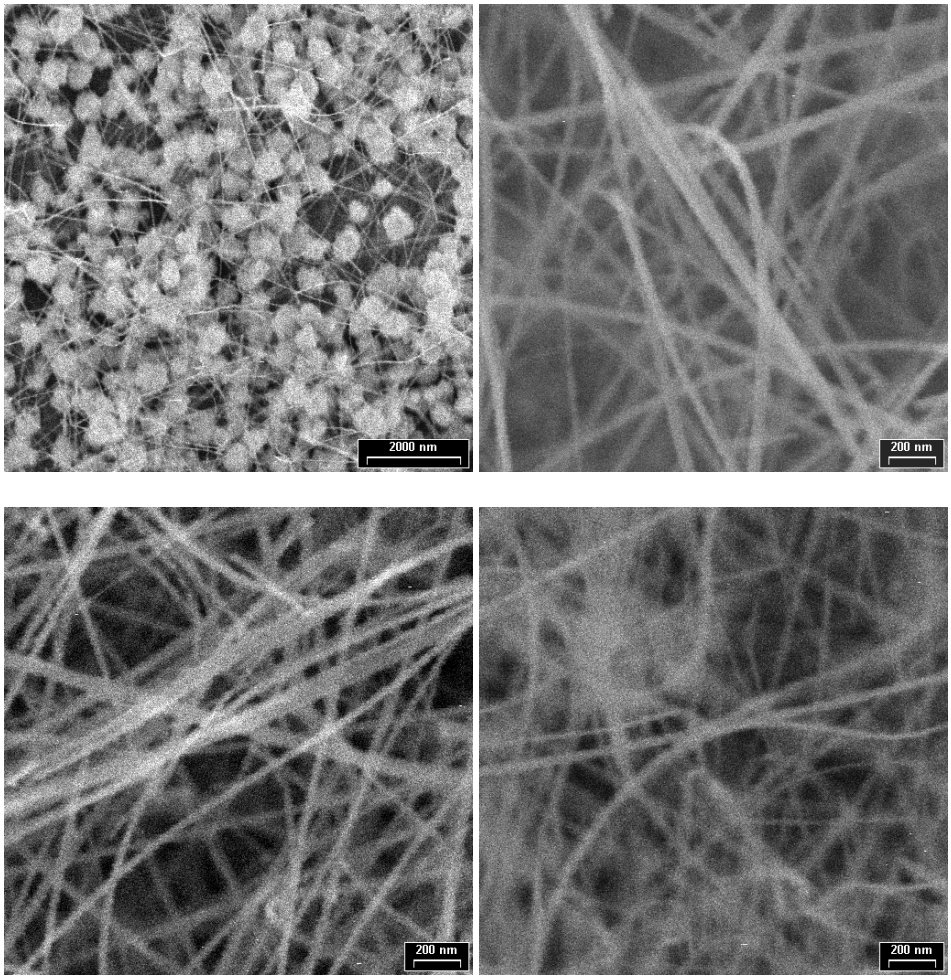

Figure 27. High density ZnO nanowires grown on the top of FTO glass substrate after extending growth time to 80 min. (a) The ZnO nanowires were grown from the nanoparticle seed sites. (b, c, d) The ZnO nanowires showed uniform geometry and have the dimensions of 30 to 40 nanometers in diameter and 1 to 2 microns in length.

With increasing the growth time, the nanowires grew longer and longer. Figure 28 shows a typical morphology of the as-synthesized ZnO nanowire after 100 min. The ZnO nanowires have an average diameter a 40 to 60 nanometers and a length is up to 4 microns. Compared to those grown for a shorter time, the average diameter did not change significantly, indicating the growth time has a little influence on the diameter of the nanowires.

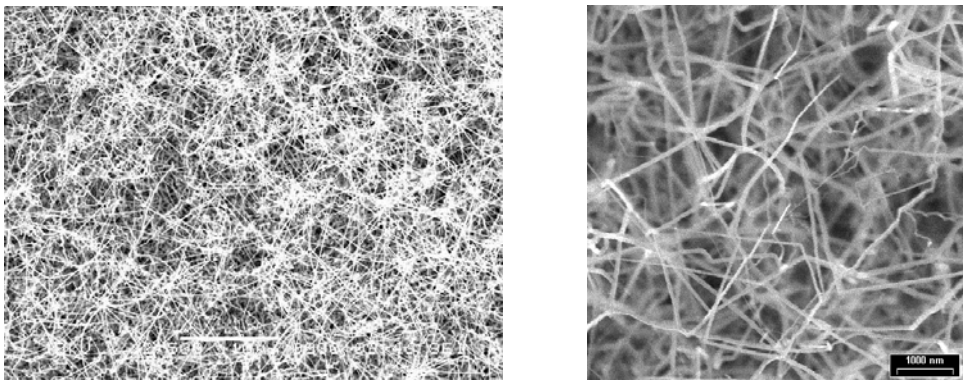

Figure 28. Typical morphology of the as-synthesized nanowires after 100min growth at 950^{o}C. (a) The ZnO nanowires grew longer as the time increasing. (b) The averaged diameter did not change significantly indicates that the growth time has litter influence on the diameter of nanowires.

When the reaction time increased up to 120 minutes, the longest ZnO nanowire is found to be approximately 4 microns as shown in Figure 29. However, for these long times, the nanowires were not evenly nor densely distributed. The exact reason why the number of synthesized nanowires decreased after 120 min growth requires further investigation. One assumption is that due to the long growth time at very high temperature, most of synthesized nanowires may have been evaporated; only the longest ones survived. In summary, the SEM data proved that the longer reaction time produced nanowires with longer length.

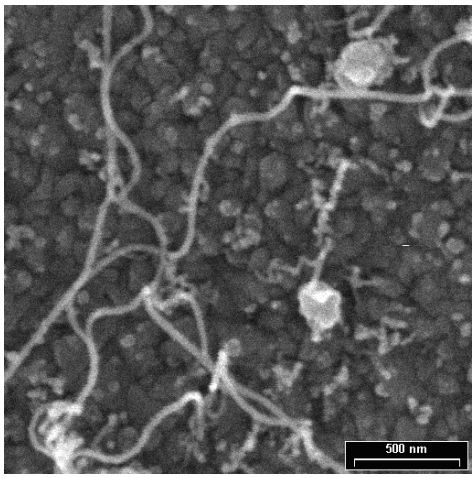

Figure 29. The length of ZnO nanowire is extended up to several microns after 120 min growth

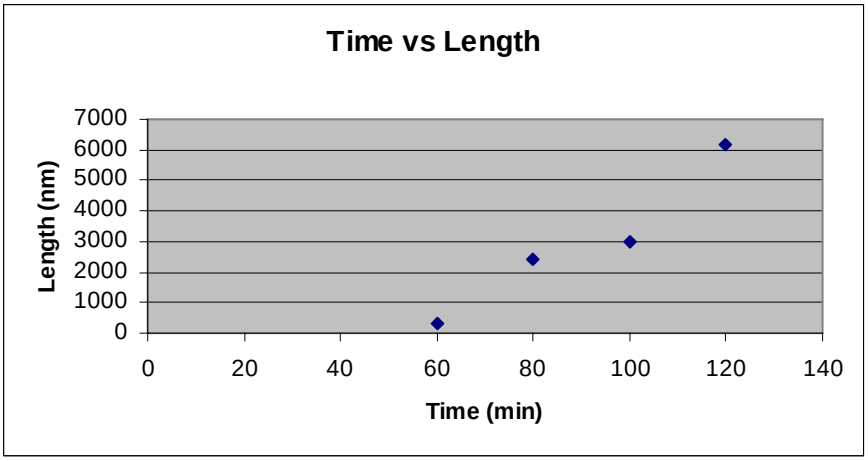

Figure 30. The dependence of ZnO nanowire length on the reaction time

Figure 30 illustrates the dependence of average length of synthesized ZnO nanowire on the reaction time. ZnO particles (rather than nanowires) were formed for reaction times less than 60 minutes in the vapor trapping CVD method. As the reaction time increased while the furnace temperature and argon gas flow rate remain unchanged, the ZnO atoms in vapor phase self-assemble into ZnO nanowires at each nucleation sites. Therefore, the ZnO nanowires were formed and grew longer and longer at their initial growth orientation.

5.2.1.2 Effect of reaction time on Diameter

The influence of reaction time on average diameter of ZnO nanowire has also been studied. The ZnO nanowires deposition processes were conducted at 950^{o}C for 60, 80, 100 and 120 minutes. Figure 31 below illustrates the dependence of ZnO nanowire average diameter on the reaction time. A slight increase in the average ZnO nanowire diameter at longer reaction time is probably due to an increase in the size of nucleation sites during the growth. For the ZnO nanowires that started to growth after 80 minutes, the diameter for as-synthesized ZnO nanowires are ranged from 30-65 nm.

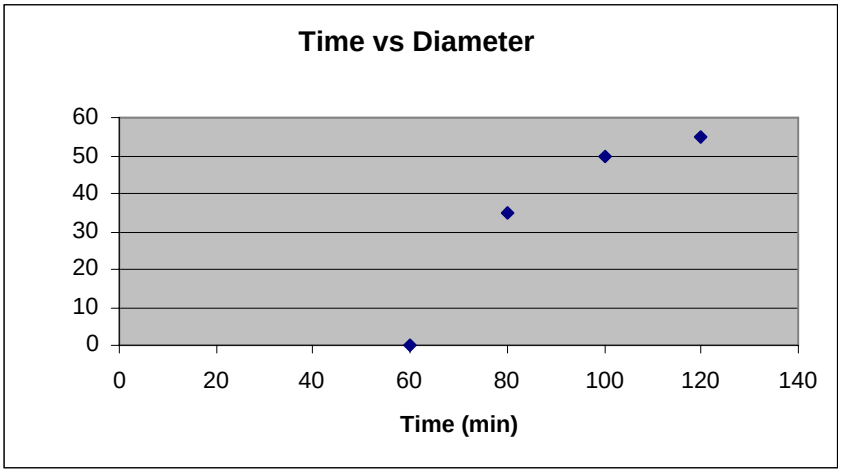

Figure 31. The dependence of ZnO nanowire diameter on the reaction time

5.2.2 Effect of reaction temperature on the morphology and density of ZnO nanowires

The effects of reaction temperature on the morphology and number density of synthesized ZnO nanowires have also been investigated. The number density of the ZnO nanowires can be defined as the number of nanowire per unit area. The second group of experiments was carried out under 70 sccm argon flow rate and the reaction time was 100 minutes. ZnO nanowires have been synthesized at different reaction temperature of 910^{o}C, 930^{o}C, 940^{o}C, 950^{o}C and 1000^{o}C to investigate the influence of temperatures on the morphology of as-synthesized products. A mixture of commercial ZnO and graphite powders in a certain ratio (1:1 by weight) was placed in the inlet vial as the source material. An FTO glass substrate was placed downstream to collect the synthesized products. All of the substrates were sputter coated with gold thin film as catalyst layer. Since the SnO_2 (Tin Dioxide) has a melting point at 1630^{o}C, the SnO_2 thin film was remains in the solid phase during the experiments.

The morphology, chemical composition and optical property of the as-synthesized nanostructures were characterized by means of scanning electron microscopy (SEM), electron dispersive X-ray spectroscopy (EDS) and photoluminescence.

Figure 32 shows the morphology of ZnO nanowire synthesized at 910^{o}C. ZnO wire-like structures were grown at the edge of each nucleation sites. The as-synthesized nanostructures were sparsely distributed on the FTO substrate surface with average length only 200-300 nm. The ZnO crystal growth rate and nucleation rate were determined by the Zn and O_2 vapor concentration ratio inside the inlet quartz vial. The evaporation rate of ZnO at 910^{o}C is limited; therefore, the number density of as-synthesized nanowires is low and the averaged length is also small.

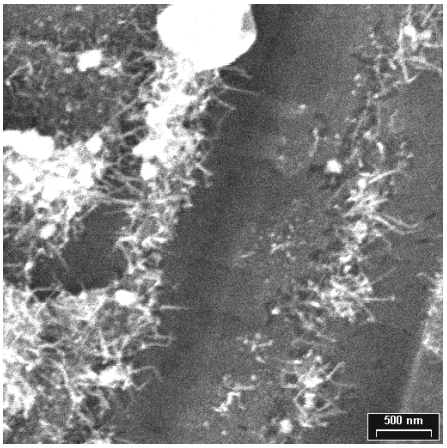

Figure 32. Morphology of the nanowires grown at 910^{o}C

When the synthesis took place at temperature of 930^{o}C for 100 minutes, typical ZnO nanowires can be seen on the substrate. As shown in Figure 33, the ZnO nanowire diameter ranged from 70 to 90 nm, the length was up to 2 to 3 microns, also with a higher aspect ratio. The argon gas flow rate was same as the growth at 910^{o}C, which is 70 sccm. It can be seen that denser ZnO nanowire were synthesized at a higher temperature condition.

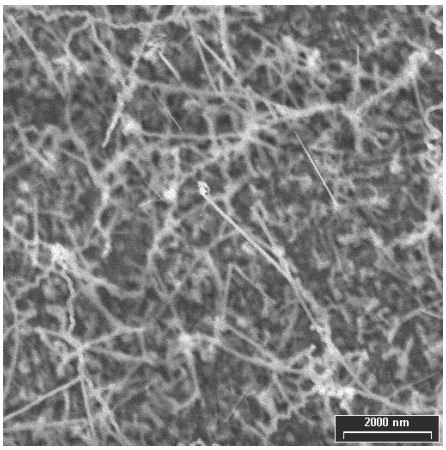

Figure 33. Typical ZnO nanowire grown at 930^{o}C

With increasing reaction temperature, more high quality ZnO nanowires were synthesized. Figure 34 illustrates the morphology of the as-synthesized ZnO nanowire grown at 940^{o}C with all the other experimental parameters unchanged. Most of the ZnO nanowires have a diameter of 50-60 nm, and their length was 3 to 4 microns, suggesting that longer and thinner ZnO nanowires can be formed by elevating reaction temperature. The SEM image indicates that average distance between each single ZnO nanowires synthesized at 940^{o}C is around 50 to 100nm.

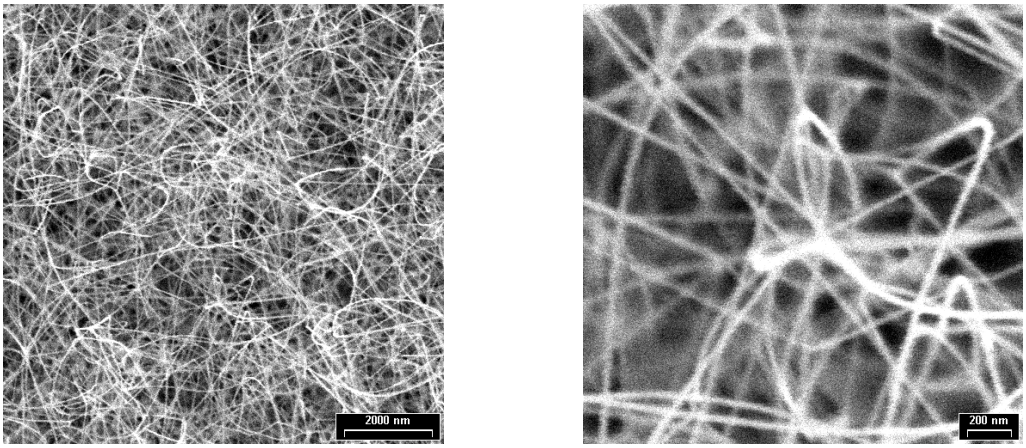

Figure 34. Dense ZnO nanowire grown at 940^{o}C

Even denser and thinner ZnO nanowires have been synthesized at 950^{o}C. As shown in Figure 35, the as-synthesized nanowires have an average diameter of 30-50 nm. The SEM data suggests that thinner ZnO nanowires can be synthesized by elevating the growth temperature and the length was also extended up to 4-5 microns.

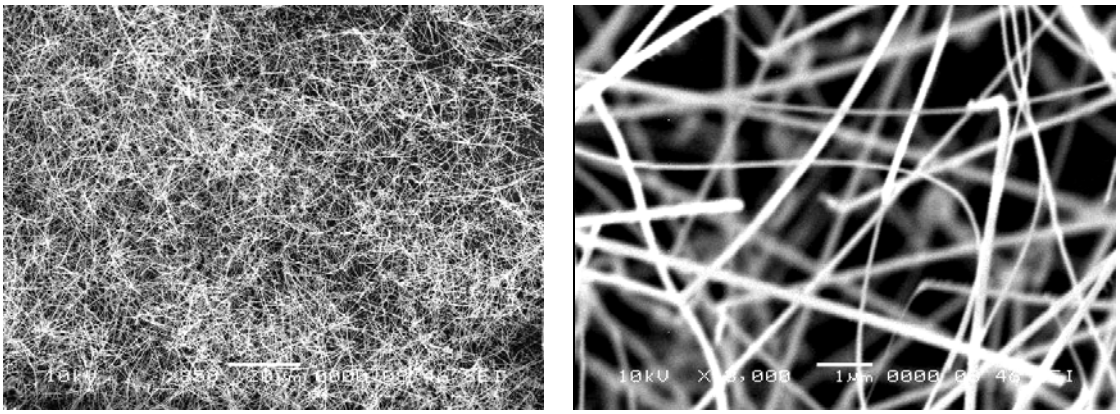

Figure 35. ZnO nanowire grown at 950^{o}C

ZnO nanowires were deposited even at the temperatures as high as 1000 ^{o}C. Figure 36 reveals the typical morphology. As shown in the SEM images, nanowires were closed spaced with average wire-to-wire distance less than 120 nm. The average diameter was still 30-50 nm, which is almost the same with the nanowires synthesized at 950^{o}C, indicating the smallest diameter can be achieved by elevating the growth temperature in the vapor trapping CVD mechanism. However, the average length has decreased to 1~2 microns. The exact reason is still not well understood, an assumption is that since the furnace temperature is as high as 1000^{o}C, dense nanowires may entangled together. Therefore, measuring the average length seems difficult.

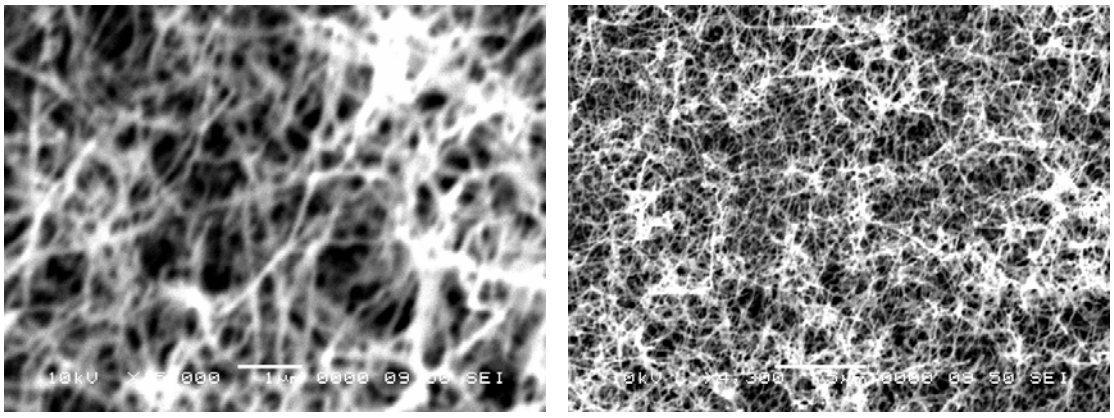

Figure 36. ZnO nanowires synthesized at 1000°C

Figure 37 illustrates the dependence of ZnO nanowire diameters on growth temperature. Basically, smaller catalyst sites, formed in the heating process, should favor the growth of thinner nanowires. In addition, the SEM data suggests that the number density of as-synthesized ZnO nanowires is controlled by the growth temperature. Nanowires grown in higher temperature have smaller wire-to-wire space, indicating denser nanowires growth.

Figure 38 illustrates the dependence of ZnO nanowire lengths on growth temperature. Longer nanowires grow more favorably to grow at higher temperatures, indicating the growth temperature will also affect the average length of ZnO nanowires.

Since the ZnO nanowires are being produced to serve as the electron accepting layer in an organic hybrid solar cell, efficient charge separation in nanowire-based architecture requires that the nanowires must thin (＜50nm) and closely spaced, with a wire-to-wire distance equal to approximately twice the diffusion length of excitons in the polymer. Therefore, the average space between each single nanowire should equal or approache to 50 nm. [54] The ZnO nanowires arrays synthesized at 950°C and 1000°C feature a

diameter, length, and density that make them quite suitable as the organic scaffold in efficient nanowire-polymer solar cells.

The SEM data suggests that growth temperature determines the morphology of as-synthesized nanostructures. ZnO nanowires favor to grow at the furnace temperature above 930^{o}C. In vapor trapping CVD mechanism, crystal growth rate is determined by zinc and oxygen vapor concentration ratio, zinc oxide nanowires can only be deposited when the Zn/O_2 vapor concentration ratio reaches a certain value. Because synthesis was conducted at 1 atm, high concentration of zinc vapor was maintained inside the vial, creating a rich zinc environment. Therefore, the higher furnace temperature yields a higher zinc oxide evaporation rate, thereby results in densely distributed nanowires.

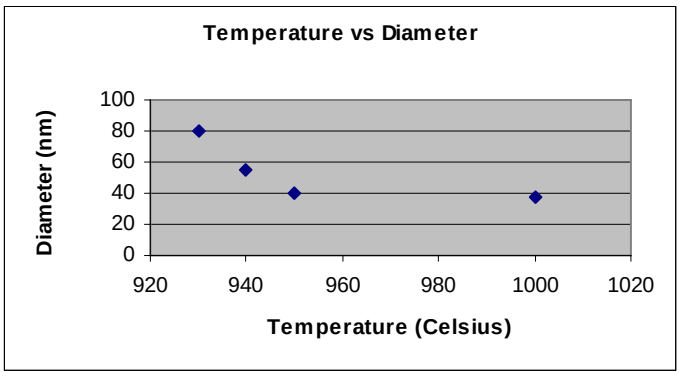

Figure 37. The dependence of ZnO nanowires diameter on growth temperature

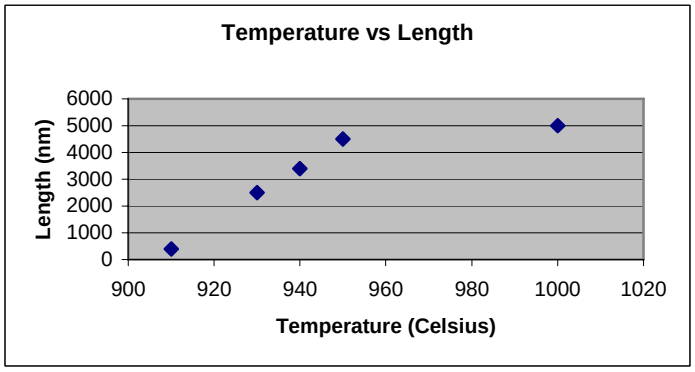

Figure 38. The dependence of ZnO nanowires length on growth temperature

Energy-dispersive X-ray spectroscopy (EDX) data acquired from ZnO nanowires grown at 950^{o}C are shown in Figure 39. These confirm that the nanowires are composed of Zn and O elements. The appearance of Si and Sn is due to the FTO glass substrate. Since the glass was coated with Tin Oxide film, the additional atomic weight of Oxygen is attributed to Silicon Oxide and Tin Oxide. According to the EDX measurement, the percentage of Oxygen atom (59.78%) is approximately equals to the sum of three kinds of oxides: ZnO, SnO_2 and SiO_2 (60.15%). This result also reveals that as-synthesized ZnO nanowires have more oxygen vacancies and zinc interstitials, which are *n*-type donors.

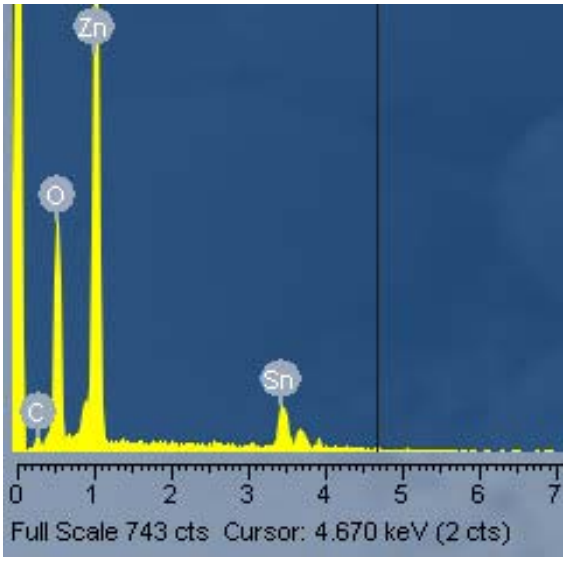

Elt	XRay	Int	Error	K	Kratio	W%	A%	ZAF	Formula	Ox%	Cat#
O	Ka	69.1	0.7586	0.0720	0.0516	23.67	59.78	4.5860		0.00	0.00
Si	Ka	64.1	0.7310	0.0311	0.0223	4.66	6.71	2.0882		0.00	0.00
Zn	Ka	139.2	1.0772	0.4334	0.3107	32.83	20.29	1.0568		0.00	0.00
Sn	La	264.5	1.4846	0.4635	0.3323	38.84	13.22	1.1688		0.00	0.00
				1.0000	0.7169	100.00	100.00			0.00	0.00

Figure 39. EDX analysis showing the nanowires are composed of Zn and O elements

5.2.3 Effect of carrier gas flow rate on density of zinc oxide nanowires

The effect of carrier gas flow rate on the density of synthesized ZnO nanowires has also been investigated. The experiments were conducted at carrier gas flow rates of 70; 139 and 200 sccm respectively, while the furnace temperature was 950^{o}C and reaction time was 100 minutes. The figure 40 shows the typical nanowires synthesized under a carrier gas flow rate of 139 sccm.

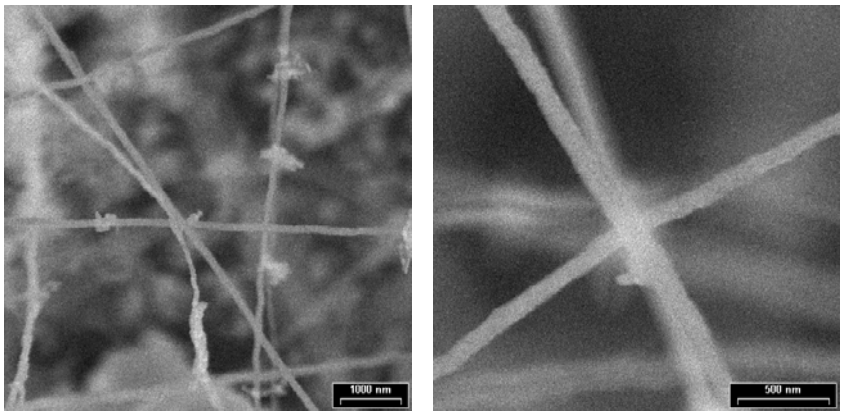

Figure 40. ZnO nanowires synthesized under the carrier gas flow rate of 139 sccm

It can be seen that only a few of nanowires have been synthesized. Compared to the nanowires synthesized under the carrier gas flow rate of 70 sccm, the density decreased significantly.

Zinc Oxide nanoparticles rather than nanowires have been synthesized under the carrier gas flow rate of 200 sccm (Fig. 41). Therefore, typical zinc oxide nanowires can be synthesized under the carrier gas flow rate around 70 sccm. If the gas flow is too strong, the rate of zinc vapor diffusing from the inlet vial will be increased, it will destruct the zinc-rich environment; thereby decrease the zinc oxide nanowire synthesis.

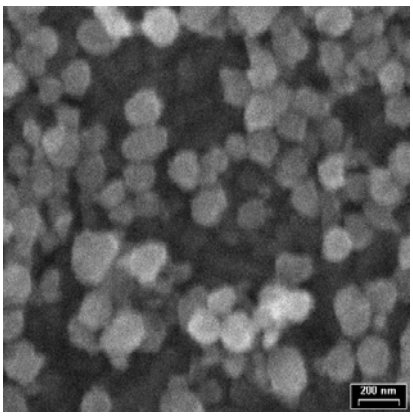

Figure 41. ZnO nanoparticles synthesized under carrier gas flow rate of 200 sccm

5.3 Hydrothermal growth of nanowires

5.3.1 Zinc oxide seed-layer preparation

Two chemical methods were evaluated for the zinc oxide dense layer preparation (see section 4.1.2.1 for details), including the dip-coating and the spin-coating. Figure 42 (a) shows the film prepared by the spin-coating method. It is obvious from the image that ZnO particles were sparsely covered the substrate. In order to have a better film, different ZnO precursor concentration and spin velocities were tested. However, pinholes were always present in these films indicating poor film coverage.

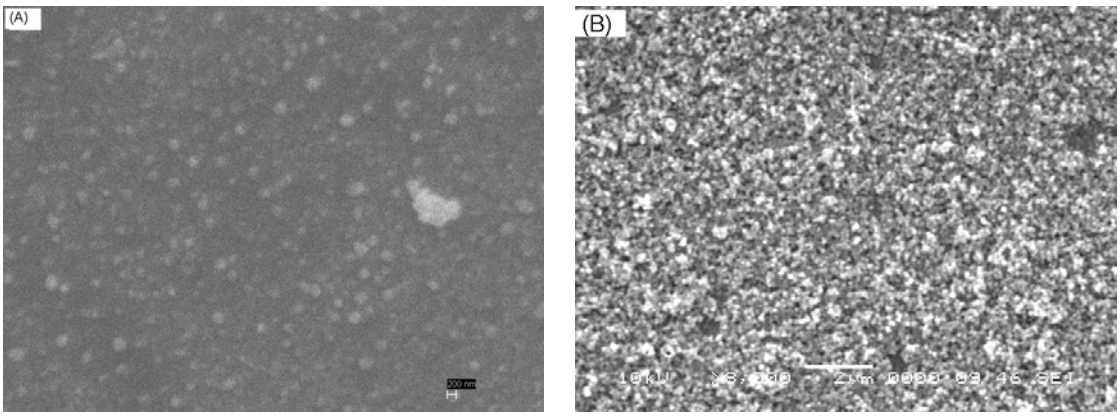

Figure 42. SEM images of ZnO seed layer studies (a) spin-coated ZnO layer (b) Dip-coated layer

For dip-coating method, different solvents (including dimethylformamide, methanol and acetone) and different concentrations of the ZnO precursor were investigated. It has been proved that methanol was the best solvent for ZnO dissolution; well-adhered films were obtained with most concentrated solutions, using methanol as a solvent.

5.3.2 Growth of ZnO nanowires onto ZnO seed-layer

ZnO nanostructures were prepared on dip-coated ZnO seed layer through two hydrothermal approaches (see section 4.1.2.2 for details). The seed layer has two

functions: (1) A hole blocking layer in solar cell architecture (2) A seed-growth layer for the ZnO nanowires/nanorods. Figure 43 shows the SEM images of the nanostructures produced from these two methods.

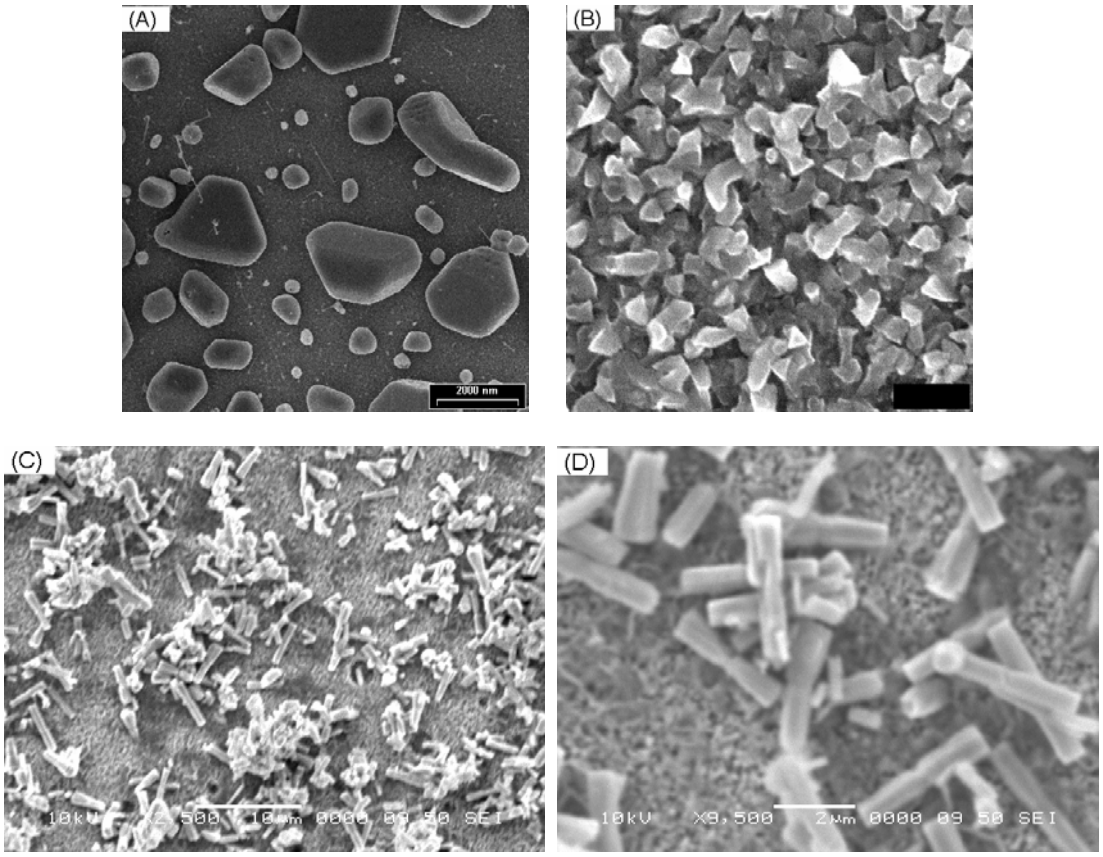

Figure 43. SEM images of ZnO nanostructures grown on dip-coated ZnO seed layer by different methods: (A) Method 1 (B) Method 2 at pH=9 scale bar: 500 nm (C) and (D) Method 3 at pH=7

Method 1 has been conducted in different growth time ranging from 3-12 hours at 60^{o}C. However, these attempts were unsuccessful, no wire-like nanostructures synthesized. Figure 40 (A) is a typical SEM image of 6 hours deposition. Obviously, ZnO chunks rather than nanowires nor nanorods were formed.

In Method 2, experiments were started with different initial pH value, from 7 to 9. Rod-like structures have been seen from the SEM images. Figure 43 (B) shows the ZnO rod-like structure synthesized at initial pH=9. The size of these rod-like structures was

uniform, 100-150 nm in average diameter and 500-700 nm in length, with aspect ratio ranging from 4 to 6. Figure 43 (C) and (D) shows the morphology of ZnO rod-like structure synthesized at initial pH=7. The shape of those structures was quite identical, with average rod diameter around 400 nm, length around 2 μm and aspect ratio about 5.0. EDX data verified that the products were mainly composed of Zinc and Oxide elements, as shown in the Figure 44 below.

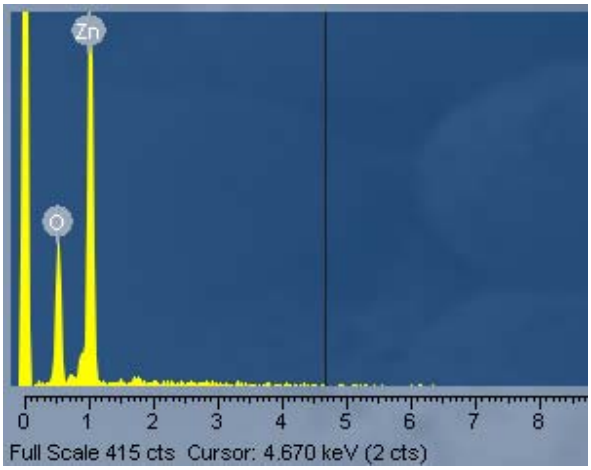

Figure 44. EDX data for hydrothermal synthesis of ZnO nanostructures.

5.4 I-V measurement of Solar cells

The bilayer CVD-grown ZnO nanowire/PTEBS polymer solar cells were tested in the dark and under AM 1.5 illuminations; the light intensity was about 80 mW/cm^2. As shown in Figure 45, the device has open circuit voltage about 0.3V, and the shape of the curve indicates diode behavior.

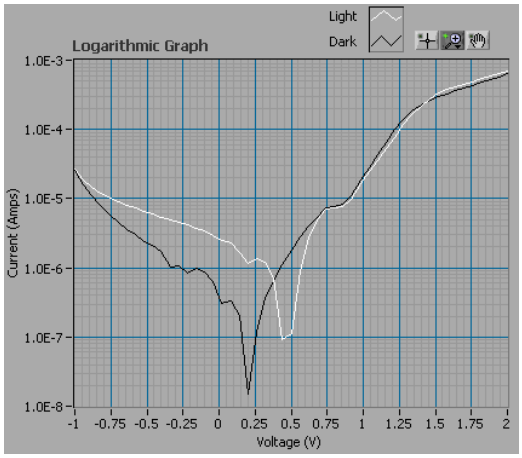

Figure 45. Current density vs applied voltage of the device tested under AM 1.5 illumination on semi-log scale

Figure 46 shows the linear current-voltage curve. However, the short circuit current was almost negligible, indicating poor carrier transport. Since the surface of ZnO samples are not quite smooth, the pits are formed on ZnO film surface. The PTEBS layers was not compact enough prevent the contact between the ZnO pits and the gold electrodes. Therefore, the devices were "shorted".

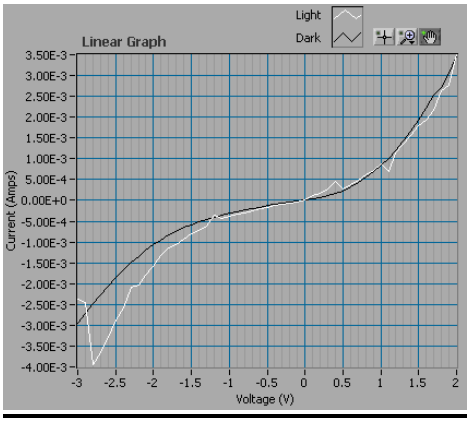

Figure 46. The linear *I-V* curve of bilayer ZnO nanowire/PTEBS polymer solar cells

One solution for the problem mentioned above is to add a PEDOT:PSS polymer layer on top of the PTEBS layer. PEDOT: PSS is a hole conducting polymer, it will prevent the electron transport to gold electrodes, while enhancing the hole transport. Figure 47 shows the I-V curve after PEDOT:PSS deposition. It shows a more pronounced diode behavior, but still a small short circuit current density of (~2 x 10^{-2} mA/cm^2) and open circuit voltage (~0.3V). Possible reasons for the poor performance are discussed in the conclusions.

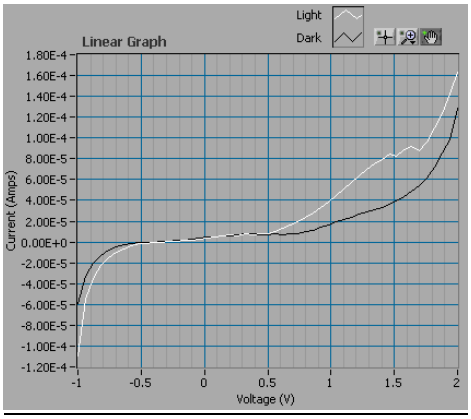

Figure 47. The linear I-V curve of bilayer ZnO nanowire/PTEBS polymer solar cells after PEDOT:PSS deposition

Chapter 6 Conclusion

Zinc oxide, a widely utilized semiconductor material, has the potential to be integrated into nanoscale electronics and photovoltaics. A modified vapor-trapping CVD method has been developed to synthesis zinc oxide nanowires. Scanning electron microscopy observations showed the morphology and density changes of zinc oxide nanowires synthesized in different environments. Therefore, the morphology and density of nanowires can be rationally manipulated by in-situ changing the synthesis parameters.

The CVD system used in this work has several controllable parameters including furnace temperature, carrier gas flow rate and reaction temperature. By adjusting one of these parameters while have the other parameters unchanged during the growth process, parametric studies of the effects of controllable factors on the morphology of chemical vapor deposition (CVD) synthesized zinc oxide nanowires have been conducted.

Basically, typical zinc oxide nanowires can be synthesized with the growth time longer than 80 minutes, and the length of nanowires is mainly determined by the growth time. At the earlier stage of the growth, gold catalyst droplets were formed at the substrate. Gaseous zinc atoms reacted with oxygen and dissolved into catalyst sites, forming zinc oxide nanoparticles. The nanoparticles served as nucleation sites for the future zinc oxide deposition, the gaseous zinc atoms continue self-assembled into nanowires at each of nucleation sites. Therefore, with the growth time increases, the nanowires grew longer and longer in a favorable growth orientation. As the growth time reached to 120 minutes, the longest zinc oxide nanowires have been produced with

average length expanded to 6 microns. In addition, Scanning electron microscopy data suggested that the diameter of zinc oxide nanowires increased slightly at the longer growth time. This might due to the increase in the size of nucleation sites during the growth.

Effect of growth temperature on morphology of zinc oxide nanowires has also been investigated. Zinc oxide nanowires can not be formed unless the growth temperature is higher than 930^{o}C. The average diameter and number density of nanowires array can be controlled by the growth temperature. The scanning electron microscopy data indicated that nanowire diameters are inversely proportional to the growth temperature; the smallest nanowires can be obtained at 950^{o}C, which is around 40 nm in diameter. Nanowires synthesized at 950^{o}C and 1000^{o}C have similar size, indicating 40 nm diameter is the smallest size that can be achieved in this CVD mechanism. This is due to the fact that smaller catalyst sites can be formed at higher temperature, smaller catalyst site should favor the thinner nanowires growth. In addition, the average diameter of synthesized nanowires decreased slightly with the rise of growth temperature.

It has been proven by previous experiments that the vapor-trapping design is critical for the nanowires synthesis. Nanowires were hard to deposit on top of the substrate without the inlet vial. Therefore, the zinc vapor concentration plays an important role during the growth process. Since the experiments were conducted at 1 atm, zinc vapor was hard to diffuse from the vial; a zinc-rich environment has been maintained inside of the vial. Zinc oxide powder evaporated quickly at higher furnace temperatures, rendering higher zinc vapor concentration. Therefore, more nanowires can be formed in a zinc-rich

environment. This is an explanation of the formation of the dense nanowires array in higher growth temperature.

Carrier gas flow rate is another factor which affects the zinc oxide nanowire number density. Argon gas has been selected as the carrier gas in this study because it is inert. Scanning electron microscopy observations reveal that typical zinc oxide nanowires can only be synthesized under the carrier gas flow rate around 70 sccm. Nanoparticles rather than nanowires were formed if the flow rate was too high.

In addition, hydrothermal synthesis of zinc oxide nanowires has also been investigated to evaluate the effect of pH on the morphology of nanowires. However, the attempts were not successful; the synthesized structures showed the rods-like shape, but the size was not in the "nano" regime.

Water-soluble polymer PTEBS and zinc oxide nanowires have been incorporated into novel bilayer organic solar cells. The results indicated that the zinc oxide nanorods grown using CVD have the potential to serve as the electron acceptor in polymer solar cells when used with the water-soluble polymer PTEBS. The device *I-V* measurement showed typical diode behavior, but the short circuit current was very low. In brief, several issues interfere with the consistent fabrication consistent of efficient devices:

1. It is difficult to deposit uniform layers of the water-soluble polymer as it tends to "bead".

2. The surface of zinc oxide nanowire samples was not flat; pits were presented in these samples. Devices based on zinc oxide nanowires maybe "shorted".

3. Due to the size limitation, using CVD to creating uniform arrays of ZnO large enough to make macroscopic devices is challenging as well.

Literature Cited

Literature Cited

[1] Zhiyong Fan and Jia G. Lu, *Zinc Oxide Nanostructures: Synthesis and Properties*. Journal of nanoscience and nanotechnology. **2005**.

[2] Y.W.Heo,L.C.Tien, D.P.Norton, and S.J.Pearton, *Pt/ZnO nanowire Schottky diodes.* Applied Physics Letters. 2004.**85**(15): p.3107-3109.

[3] H.Kind, H.Yan, B.Messer, M.Law, P.Yang, *Nanowire Ultraviolet Photodetectors and Optical Switches.* Advanced Materials. 2002. **14**(2): p.158-160.

[4] Zhiyong Fan and Jia G. Lu, *Gate-refreshable nanowire chemical sensors.* Applied Physics Letters. **86**. 123510 (2005).

[5] Peiro, A.M., et al., *Hybrid polymer/metal oxide solar cells based on ZnO columnar structures.* Journal of Materials Chemistry, 2006. **16**(21): p. 2088-2096

[6] Beek, W.J.E., M.M.Wienk, and R.A.J. Janssen, *Efficient hybrid solar cells from zinc oxide nanoparticles and a conjugated polymer.* Advanced Materials, 2004. **16**(12): p. 1009-1013

[7] Baigent, D.R.,et al., *Conjugated Polymer Light-Emitting-Diodes on Silicon Substrates.*Applied Physics Letters, 1994. **65**(21): p.2636-2638.

[8] Baraton, M.I., et al., *Inverstgation of the TiO_2/PPV nanocomposite for gas sensing applications.* Nanotechnology, 1998. **9**(4): p.356-359.

[9] Qiao,Q., et al., *Characteristics of Water Soluble Polythiophene: TiO_2 Composite and its Application in Photovoltaics.* Journal of Applied Physics, 2005. **98**(10): p.094906.

[10] C. Klingshirn, *ZnO: Material, Physics and applications.* Chemical Physics and Physical Chemistry 2007. **8**(6): p. 782-803.

[11] The structure of Materials: The website of Carnegie Mellon University. http:// som.web.cmu.edu

[12] Zhonglin Wang, *Zinc oxide nanostructures: growth, properties and applications.* Journal of Physics: Condensed Material. 2004. **16:** p.R829-R858.

[13] G.Ali Mansoori, *Principles of Nanotechnology: Molecular-Based Study of Condensed Matter in Small Systems.* Published by World Scientific, 2005. p.4-6.

[14] P.M. Mathews and K. Venkatesan; *Quantum Mechanics*. Edition 36. Published by Tata McGraw-Hill, 1978.

[15] Zhonglin Wang. *Nanowires and Nanobelts: Materials, Properties and Devices, Metal and Semiconductor Nanowires*. Volume I. Published by Kluwer Academic, 2005.

[16] S.J. Tans, R.M. *Verschueren and C.dekker, Room-temperature transistor based on a single carbon nanotube.* Nature.1998. **393:** p. 49-52.

[17] Z.Yao, H.W.C. Postma, L. Balents and C.Dekker, *Carbon nanotube intramolecular junctions.* Nature. 1999. **402:** p.273-276.

[18] V.Derycke, R. Martel, J.Appenzeller and P. Avouris, *Carbon Nanotube Inter- and intramolecular Logic Gates.* Nano Letters, 2001. **1**(9): p. 453-456.

[19] X.Duan and C.M.Lieber, *General Synthesis of Compound Semiconductor Nanowires.* Advanced Material. 2001. **12**(4):p.298-302

[20] X.Duan, Y Huang, Y.Cui, J. Wang and C.M. Lieber, *Indium phosphide nanowires as building blocks for nanoscale electronic and optoelectronic devices.* Nature 2001. **409:** p. 66-69.

[21] Y.Cui and C.M.Lieber, *Functional Nanoscale Electronic Devices Assembled Using Silicon Nanowire Building Blocks.* Science. 2001. **291**(5505): p.851-853.

[22] Y.Huang, X. Duan, Y.Cui, L. Lauhon,K.Kin and C.M.Lieber, *Logic Gates and Computation from Assembled Nanowire Building Blocks.* Science 2001.**294**(5545): p.1313-1317.

[23] X. Wang, Y. Ding, C. J. Summers, Z. L. *Wang, Large-Scale Synthesis of Six-Nanometer-Wide ZnO nanobelts*. Journal of Physical Chemistry.2004.**113**(24): p. 6537-6539.

[24] J. W. Chiou, K. P. Krishna Kumar, J. C. Jan, H. M. Tsai, C. W. Bao, W. F. Pong, F. Z. Chien, M.-H. Tsai, I.-H. Hong, R. Klauser, J. F. Lee, J. J. Wu, and S. C. Liu, *Diameter dependence of the electronic structure of ZnO nanorods determined by x-ray absorption spectroscopy and scanning photoelectron microscopy.* Applied Physics Letters. 2004 **85**(15): p.3220-3222.

[25] H. Chik, J. Liang, S. G. Cloutier, N. Kouklin, J. M. Xu, *Periodic array of uniform ZnO nanorods by second-order self-assembly.* Applied. Physics. Letters. 2004 **84**(17):. p.3376-3378.

[26] X.D.Bai, P.X.Xiao and Zhonglin Wang, *Dual-mode mechanical resonance of individual ZnO nanobelts.* Applied Physics Letters.2003. **82**(26): p. 4806-4808.

[27] H. G. Craighead. *Nanoelectromechanical System.* Science 2000. **290**(5496): p.1532-1535.

[28] Zhao M H, Wang Z L and Mao S X. *Piezoelectric Characterization of Individual Zinc*

Oxide Nanobelt Probed by Piezoresponse Force Microscope. Nano Letters. 2004. **4**(4)**:**587-590.

[29] P. Chang, Z. Fan, W. Tseng, D. Wang, W. Chiou, J. Hong, J. G. Lu, *Zinc Oxide Nanowires Synthesized by Vapor Trapping CVD Method.* Chemistry of Materials. 2004. **16:** 5133-5137.

[30] W. I. Park, J. S. Kim, G.-C. Yi, M. H. Bae, H.-J, Lee, *Fabrication and electrical characteristics of high-performance ZnO nanorods field-effect transistors.* Applied Physical Letters. 2004. **85**(21): p.5052-5054.

[31] D. C. Look, D. C. Reynolds, C. W. Litton, R. L. Jones, D. B. Eason, G. Cantwell, *Characterization of homoepitaxial p-type ZnO grown by molecular beam epitaxy.* Appied. Physicsl Letters. 2002. **81**(10): p.1830-1832.

[32] K.-K. Kim, H.-S. Kim, D.-K. Hwang, J.-H. Lim, S.-J. Park, *Realization of p-type ZnO thin films via phosphorus doping and thermal activation of the dopant.* Applied Physics Letters. 2003. **83**(1): p.63-65.

[33] C. H. Liu, W. C. Yiu, F. C. K. Au, J. X. Ding, C. S. Lee, S. T. Lee, *Electrical properties of zinc oxide nanowires and interamolecular p-n junctions.* Applied Physics Letters. 2003 **83**(15): p.3168-3170.

[34] Huang M H, Mao S, Feick H, Yan H Q, Wu Y Y, Kind H, Weber E, Russo R and Yang P D, *Room-Temperature Ultraviolet Nanowire Nanolasers.* Science. 2001 **292**(5523): p.1897-1899,

[35] M. Catti, Y. Noel, and R. Dovesi, J. *Full piezoelectric tensors of wurtzite and zinc blende ZnO and ZnS by first-principles calculations.* Journal of physics and Chemistry of Solids. 2003.**64**(11): p.2183-2190.

[36] J.G.E. Gardeniers,Z.M. Rittersma, and G.J.Burger, *Preferred orientation and piezoelectricity in sputtered ZnO films.* Journal of Applied Physics. 1998. **83**(12): p.7844-7854.

[37] H.-W. Ryu, B.-S. Park, S. A. Akbar, W.-S. Lee, K.-J. Hong, Y.-Jin Seo, D.-C. Shin, J.-S. Park, G.-P. Choi, *ZnO sol-gel derived porous film for CO gas sensing.* Sensors and Actuators B. 2003. **96**: p. 717-722.

[38] G. Sberveglieri, *Recent developments in semiconducting thin-film gas sensors.* Sensors and Actuators B. 1995.**23:** p.103-109.

[39] G.S.Trivikrama Rao, D. Tarakarama Rao, *Gas sensitivity of ZnO based thick film sensor to NH_3 at room temperature.* Sensors and Actuators B. 1999. **55**: p.166-169.

[40] X.L.Cheng, H.Zhao, L.H.Huo, S.Gao, J.G.Zhao, *ZnO nanoparticulate thin film: preparation, characterization and gas-sensing propertiy.* Sensors and Actuators B.2004. **102**: p.248-252.

[41] Q. Wan, Q. H. Li, Y. J. Chen, T. H. Wang, X. L. He, J. P. Li, C. L. Lin, *Fabrication and ethanol sensing characteristics of ZnO nanowire gas sensors.* Applied Physics Letters. 2004. **84**(18): p. 3654-3656.

[42] S. N. Cha, J. E. Jang, Y. Choi, G. W. Ho, D.-J. Kang, D. G. Hasko, M. E. Welland and G. A. J. Amaratunga, *High performance ZnO nanowire Field Effect Transistor.*Proceedings of ESSDERC,Grenoble, France,**2005:** p.217-219.

[43] Zhiyong Fan and Jia G. Lu. *Electrical properties of ZnO nanowire field effect transistors characterized with scanning probes.* Applied Physics Letters. 2005. **86**(3): p.032111.

[44] Jupeng Liu, Shanshan Wang, *Organic/inorganic hybrid solar cells with vertically orientated ZnO nanowires.* Applied Physics Letters. 2009**. 94** (17): p.1173107

[45] Yasuhide Nakamura, *Solution-Growth of Zinc Oxide Nanowires for Dye-Sensitized Solar Cel.* Materials**, 2006**: p.74-75.

[46] Jong-Hee Park and T.S. SUdarshan, *Chemical Vapor Deposition.* Published by ASM international. 2000.

[47] J.R.Heath, F.K.LeGoues, *A liquid solution synthesis of single crystal germanium quantum wires.* Chemistry Physics Letters. 1993. **208**(3-4): p.263-268.

[48] Jinmin Wang and Lian Gao, *Wet chemical synthesis of ultralong and straight single-crystalline ZnO nanowires and their excellent UV emission properties.* Journal of Materials Chemistry. 2003 **13**: p. 2552-2554.

[49] E. C. Greyson, Y. Babayan, and T. W. Odom, *Directed Growth of Ordered Arrays of Small-Diameter ZnO Nanowires.* Advanced Materials.2004. **16**(15): 1348-1352.

[50] H. J. Fan, F. Fleischer, W. Lee, K. Nielsch, R. Scholz, M. Zacharias, U. Gösele, A. Dadgar, and A. Krost, *Patterned growth of aligned ZnO nanowire arrays on sapphire and GaN layers.* Supperlattice Microstructures.2004.**36**(1-3). p.95-105.

[51] H. Chik, J. Liang, S. G. Cloutier, N. Kouklin, J. M. Xu, *Periodic array of uniform ZnO nanorods by second-order self-assembly.* Applied. Physics. Letters. 2004 **84**(17). p.3376-3378.

[52] P. Yang, H. Yan, S. Mao, R.Russo, J. Johnson, R. Saykally, *Controlled Growth of ZnO Nanowires and Their Optical Properties*. Advanced Material, 2002.**12**(15): p.323-331.

[53] W.I. Park, and G. C. Yi. *Electroluminescence in n-ZnO Nanorod Arrays Vertically Grown on p-GaN.* Advanced Material. 2004. **16**(1).p.87-90.

[54] H. T. Ng, J. Han, T. Yamada, P. Nguyen, Y. P. Chen, M. Meyyappan, *Single Crystal Nanowire Vertical Surround-Gate Field-Effect Transistor.* Nano Letter. 2004. **4**(7). p. 1247-1252.

[55] Wenjie Mai, Puxian Gao, Changshi Lao, Zhong Lin Wanga, Ashok K. Sood, Dennis L. Polla, Martin B. Soprano, *Vertically aligned ZnO nanowire arrays on GaN and SiC substrates.* Chemical Physics Letters. 2008. **460**. p. 253-256.

[56] Introduction to Scanning Electron Microscopy
http://en.wikipedia.org/wiki/Scanning_electron_microscope

[57] Introduction to Energy Dispersive Spectroscopy
http://en.wikipedia.org/wiki/Energy_Dispersive_Spectroscopy

[58] Qiao, Q., *Green organic solar cells from a water soluble polymer and nanocrystalline titanium dioxide*. Ph.D. Dissertation **2006**

[59]Serap Gu¨nes,* Helmut Neugebauer, and Niyazi Serdar Sariciftci, *Conjugated Polymer-Based Organic Solar Cells.* Chemistry Reviews. 2007, **107**: p. 1324-1338.

[60] The Royal Swedish Academy of Science. *The Nobel Prize in Chemistry 2000: Conductive Polymers*.
http://nobelprize.org/nobel_prizes/chemistry/laureates/2000/chemadv.pdf

[61] Harald Hoppe, Niyazi Serdar Sariciftci, *Organic solar cells: An overview.* Journals of Materials Research. 2004. **19**(7): p. 1924-1945.

[62] Kymakis, E., I. Alexandrou, and G.A.J. Amaratunga, *High open-circuit voltage photovoltaic devices from carbon-nanotube-polymer composites.* Journal of Applied Physics, **2003**. **93**(3): p.1764-1768.

[63] W Ma, C Yang, X Gong, K Lee, and A J Heeger. *Thermally Stable, Efficient Polymer Solar Cells with Nanoscale Control of the Interpenetrating Network Morphology.* Advanced Functional Materials, **2005**. **15**(10): p. 1617-1622.

[64] Qiao, Q. and J.T. McLeskey, Jr., *Water-soluble polythiphene/nanocrystalline TiO_2 solar cells*. Applied Physics Letters, 2005. **86**(15): p. 153501/1-153501/3.

[65] Patil, A.O., et al., *Water-Soluble Conducting Polymers.* Journal of the American Chemical Society, 1987. **109**(6): 1858-9.

[66] Arango, A.C., S.A. Carter, and P.J. Brock. *Charge transfer in photovoltaics consisting of interpenetrating networks of conjugated polymer and TiO_2 nanoparticles*. Appied. Physic Letters, 1999. **74**(12): p. 1698-1700.

[67] Reyes, R.R., Kim,K, and David L. Carroll. *High-efficiency photovoltaic devices based on annealed poly(3-hexylthiophene) and 1-(3-methoxycarbonyl)-propyl-1- phenyl-(6,6)C61 blends.* Applied Physics Letters. 2005, **87**(8):083506.

[68] Brabec, C.J., et al. *Organic Photovoltaics.* Springer series in Materials Science, ed. R.Hull, R.M.J. Osgood, and J.Parisi. Vol. 60. **2003.**

[69] Glenis, S., et al., *Electrochemically growth Polythiophene and poly(3-methylthiophene) organic photovoltaic cells.* Thin Solid Films, 1984, **111**(2): 93-103

[70] Marks, R.N., et al., *The photovoltaic response in poly(p-phenylene vinylene) thin-film devices.* Journal of Physics-Condensed Matter, 1994.**6**(7): p.1379-1394.

[71] Arango, A.C., et al., *Efficient Titanium Oxide/Conjugated Polymer Photovoltaics for Solar Energy Conversion.* Advanced Materials, 2000. **12**(22): p.1689-1692.

[72] Sun, S.-S. and N.S. Sariciftci, *Organic Photovoltaics: Mechanisms, Materials, and Devices*. 2005 Wiley.

[73] Tang, C.W., *Organic electroluminescent diodes.* Applied. Physic Letters. 1986**. 48**(2): p.183-185.

[74] Granstrom, M., et al., *Laminated fabrication of polymeric photovoltaic diodes.* Nature. 1998. **359**: p.257-260.

[75] Breeze, A.J., et al., *Review: Recent Advances in Organic Solar Cells.* Physical Review B (Condensed Matter and Materials Physics). 2001. **72**(4): p.125205.

[76] Huynh, W.U., X.G. Peng, andA.P. Alivisatos, *CdSe Nanocrystal Rods/Poly(3-hexylthiophene Composite Photovoltaic Devices.* Advanced Materials, 1999. **11**(11): p. 923-927.

[77] Kymakis, E. and G.A.J. Amaratunga, *Single-wall carbon nanotube/conjugated polymer photovoltaic devices.* Applied Physics Letters. 2003.**80**(4): p. 465-472.

[78] Lori E. Greene, Benjamin D. Yuhas, Matt Law, David Zitoun, and Peidong Yang, *Solution-Growth of Zinc Oxide Nanowires.* Inorganic Chemistry. 2006, **45**: p. 7535-7543.

[79] N. R. S. Farley, C. R. Staddon, L. Zhao, K. W. Edmonds, B. L. Gallagher and D. H. Gregory, *Sol-gel formation of ordered nanostructured doped ZnO films.* Journal of Materials Chemistry.2004. **14**: p. 1087-1092.

[80] Y. Natsume and H. Sakata, *Zinc oxide films prepared by sol-gel spin-coating.* Thin Solid Films, 2000. **372**(1-2): p.30-36.

[81] Greene, L.E., et al., *General Route to Vertical ZnO Nanowire Arrays Using Textured ZnO seeds*. Nano Letters, 2005. **5**(7): p. 1231-1236.

VITA

January 29, 1985	Born- Xi'an, Shaanxi, China
July 2007	B.S., Mechanical Engineering XiDian University, Xi'an, China
August 2007 – Present	Graduate Research Assistant, Nanomanufacturing Laboratory & Energy Conversion Systems Laboratory, Richmond, Virginia